Targeting inter-organ cross-talk in cardiometabolic diseases

Liu, C.

4

γ-hydroxybutyric acid attenuates diet-induced metabolic dysfunction in developing and existing obesity

Cong Liu[1,2], Mik Zwaan[1,2], Aswin Verhoeven[3], Mink S. Schinkelshoek[4], Rolf Fronczek[4], Gert Jan Lammers[4], Yanan Wang[1,2,5], Martin Giera[3], Mariëtte R. Boon[1,2], Patrick C.N. Rensen[1,2,5], Milena Schönke[1,2]

[1] Department of Medicine, Division of Endocrinology, Leiden University Medical Center, Leiden, 2333 ZA, The Netherlands.
[2] Einthoven Laboratory for Experimental Vascular Medicine, Leiden University Medical Center, Leiden, 2333 ZA, The Netherlands.
[3] Center for Proteomics and Metabolomics, Leiden University Medical Center, Leiden, 2333 ZA, The Netherlands.
[4] Department of Neurology, Division of Endocrinology, Leiden University Medical Center, Leiden, 2333 ZA, The Netherlands.
[5] Med-X institute, Center for Immunological and Metabolic Diseases, and Department of Endocrinology, First Affiliated Hospital of Xi'an Jiaotong University, Xi'an Jiaotong University, Xi'an, 710061, China.

In preparation.

ABSTRACT

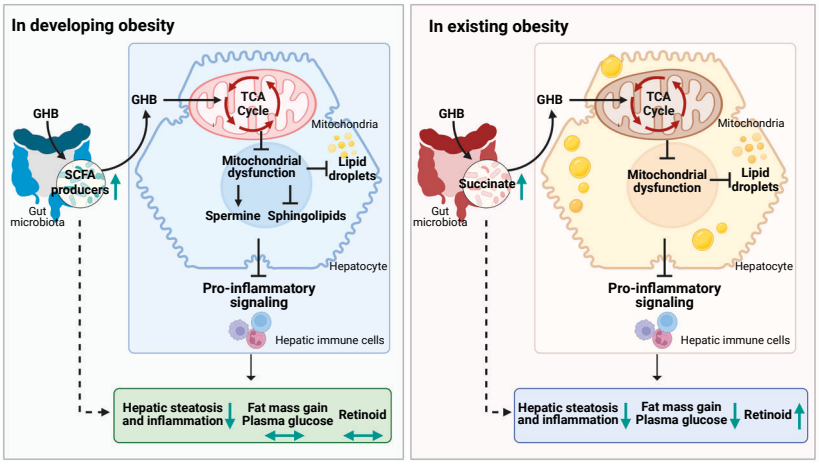

The narcolepsy drug γ-hydroxybutyric acid (GHB) promotes weight loss via unknown mechanisms. Here, we aimed to unveil the metabolic mechanisms underlying GHB-induced weight reduction in obesity. Furthermore, we aimed to examine whether GHB administration also confers weight loss during the development of obesity. We investigated the role of oral GHB treatment in body weight control in high fat diet (HFD)-induced developing and existing obesity in C57BL/6J mice. In existing obesity, but not in developing obesity, GHB attenuated HFD-induced fat mass gain, glucose intolerance and insulin resistance. However, in both metabolic conditions, GHB alleviated HFD-induced hepatic steatosis and inflammation. This was accompanied by improved hepatic mitochondrial dysfunction, as evidenced by upregulated hepatic genes encoding mitochondrial respiratory complexes. In line with this, in developing obesity, GHB alleviated the accumulation of toxic sphingolipids in the liver and in the circulation. In existing obesity, GHB prevented hepatic loss of retinoids and increased circulating acyl-carnitine, a substrate for brown fat combustion. Consistently, GHB alleviated HFD-induced adipose tissue dysfunction in obese mice, as evidenced by increased UCP-1 abundance in brown fat and decreased white adipocyte size and white fat inflammation. Moreover, GHB beneficially influenced the gut microbial composition, as shown by enrichment of short chain fatty acid producers in developing obesity, and anti-inflammatory and succinate-producers in existing obesity. Collectively, GHB promotes metabolic health in developing and existing obesity, which is associated with improved hepatic mitochondrial function, and likely involves beneficial modulation of the gut microbial composition. Our findings thus uncover previously unknown metabolic effects of GHB related to body weight management, and provide novel insights for new therapeutic handles for treating obesity and its related diseases.

INTRODUCTION

Obesity, one of the most prevalent public health concerns worldwide, is recognized as a major risk factor for the development of metabolic complications, such as type 2 diabetes (T2D) [1] and non-alcoholic fatty liver disease (NAFLD) [2]. Although lifestyle changes, medications and bariatric surgery are adopted in the clinic for body weight management [3, 4], the prevalence of obesity and its associated metabolic diseases continues to increase [4-6]. Therefore, additional therapeutics and strategies for the treatment of obesity are still needed.

Clinical studies have reported that γ-hydroxybutyric acid (GHB) treatment exerts weight loss-promoting effects [7-9]. GHB is naturally present in the mammalian brain where it acts as a neurotransmitter and neuromodulator, but it is also registered as a drug for treating the sleep disorder narcolepsy [10]. Narcolepsy commonly causes an increase in body weight after disease onset, frequently leading to obesity [11-13]. Despite being clinically used in the treatment of narcolepsy, GHB is unlikely to be prescribed as anti-obesity drug due to its central effects and its misuse-associated adverse effects (e.g. severe respiratory depression) [14]. However, elucidating the underlying mechanisms by which GHB reduces body weight may reveal therapeutic handles for the development of effective body weight control medications.

Although binding of GHB to brain-specific sites is well established and proposed to explain its neuro-biologic [10, 15] and neuro-pharmacologic properties [14, 16], the metabolic effects of GHB are speculated to be mediated by peripheral organs [17-19]. In particular, the liver is the primary organ involved in GHB metabolism [17, 20-22], as evidenced by studies showing that approximately 95-98% of administered GHB is metabolized in the liver [22, 23]. Within the liver, the major route of exogenous GHB metabolism is oxidation in the mitochondria of hepatocytes, where GHB can either directly undergo β-oxidation or can be oxidized via succinic semialdehyde to succinate. Consequently, GHB is transformed to carbon dioxide and water through the tricarboxylic acid (TCA) cycle [22].

Accumulating evidence has shown that the dysregulation of TCA cycle activity and mitochondrial function in the liver are associated with aberrant hepatocyte lipid accumulation [25, 26]. Given that the degree of liver lipid overload is directly linked to the severity of insulin resistance [27] and aberrant fat expansion [28-30], we hypothesized that GHB treatment may improve hepatic mitochondrial function to reduce hepatic lipid overload, thereby promoting weight loss. In addition, GHB is a short chain fatty acid (SCFA), and administration of the SCFAs butyrate and propionate

alleviates obesity-associated metabolic diseases at least partially through the beneficial modulation of the gut microbiota [31, 32]. Therefore, GHB treatment may also alter the gut microbial composition to exert weight loss-promoting effects.

In the present study, we tested the hypothesis that GHB administration beneficially modulates the function of the liver and/or the gut microbiota to improve obesity and its related disorders.

MATERIALS AND METHODS

Please see the **Supporting Information** for a detailed description of experimental procedures.

Animals and treatments

Male C57BL/6J mice were purchased from The Jackson Laboratory. Mice were group-housed under standard conditions (22℃; 12/12-hour light/dark cycle) with *ad libitum* access to water and rodent chow diet (Standard Rodent Diet 801203, Special Diets Services, United Kingdom), unless indicated otherwise. All animal experiments were carried out according to the Institute for Laboratory Animal Research Guide for the Care and Use of Laboratory Animals, and were approved by the National Committee for Animal Experiments (Protocol No. AVD1160020173305) and by the Ethics Committee on Animal Care and Experimentation of the Leiden University Medical Center (Protocol No. PE.18.034.042). All animal procedures were conform with the guidelines from Directive 2010/63/EU of the European Parliament on the protection of animals used for scientific purposes.

To evaluate the effects of GHB treatment on body weight control in existing obesity, we conducted a first therapeutic (T) experiment, in which 8-weeks-old mice were fed a high fat diet (HFD; 45% fat; ssniff, Soest, Germany) for 8 weeks to induce obesity. Then, based on body weight, body composition and 4-hour fasted plasma glucose and lipids, these mice were randomized into 2 groups (n = 8 per group) using RandoMice [33] to receive either GHB treatment ('T-GHB'; 150 mg/kg body weight via daily oral gavage, according to a pilot dose-finding study showing that this dosage did not cause a catatonic state in mice) or sterile-filtered water ('T-Vehicle') for 8 weeks. Moreover, to explore whether GHB administration confers weight loss effects in developing obesity, in a second preventive (P) experiment, mice at the age of 8 weeks were randomized into 2 groups (n = 8 per group). Then, they were fed a HFD while being administered with either GHB ('P-GHB'; 150 mg/kg body weight via daily oral gavage) or sterile-filtered water ('P-Vehicle') for 8 weeks.

Statistical analyses

Comparisons between two groups were performed using unpaired two-tailed Student's *t*-tests or two-way analysis of variance (ANOVA), unless indicated otherwise. Data are presented as mean ± SEM, and a *P* value less than 0.05 is considered statistically significant. All statistical analyses were performed with GraphPad Prism 9 (GraphPad Software Inc., CA, USA).

RESULTS

Oral administration of GHB attenuates fat mass gain and improves glucose control in existing obesity

To elucidate the mechanisms underlying GHB-mediated weight loss in obesity, we fed 8-week-old male wild-type C57BL/6J mice a HFD for 8 weeks to induce obesity, after which these mice continued to eat the same HFD and were treated with either vehicle or GHB for another 8 weeks (**Fig. 1A**). GHB did neither affect cumulative food intake over 8 weeks (**Fig. S1A**) nor voluntary locomotor activity (**Fig. S1B**). Nonetheless, GHB attenuated body weight gain (**Fig. 1B**), as explained by reduced gain of fat mass (**Fig. 1C**) rather than lean mass (**Fig. S1C**). Consistently, GHB reduced gonadal white adipose tissue (gWAT) and interscapular brown adipose tissue (iBAT) mass (**Fig. 1D-E**). In gWAT, GHB attenuated adipocyte enlargement (**Fig. 1F**) and reduced gene expression of the inflammatory markers adhesion G protein-coupled receptor E1 (*Adgre1*), encoding the macrophage surface marker F4/80, and tumor necrosis factor α (*Tnfa*), encoding a pro-inflammatory cytokine (**Fig. 1G**). In iBAT, GHB decreased the lipid content (**Fig. 1H**) and increased uncoupling protein-1 (UCP-1) protein abundance (**Fig. 1I**).

We next examined the modulatory role of GHB treatment in lipid and glucose metabolism. GHB had no impact on fasting plasma levels of triglycerides (TG) (**Fig. S1D**), non-esterified fatty acids (NEFA) (**Fig. S1E**) or free glycerol (**Fig. S1F**). Nonetheless, GHB did reduce fasting plasma glucose levels from four weeks of treatment onwards (**Fig. 1J**). Moreover, GHB improved glucose clearance during an intraperitoneal glucose tolerance test (**Fig. 1K**), and lowered fasting plasma insulin levels at week 6 (**Fig. 1L**). Consistently, GHB decreased the Homeostatic Model Assessment for Insulin Resistance (HOMA-IR) index (**Fig. 1M**). Collectively, these findings demonstrate that GHB attenuates diet-induced fat mass gain and improves glucose homeostasis in obesity.

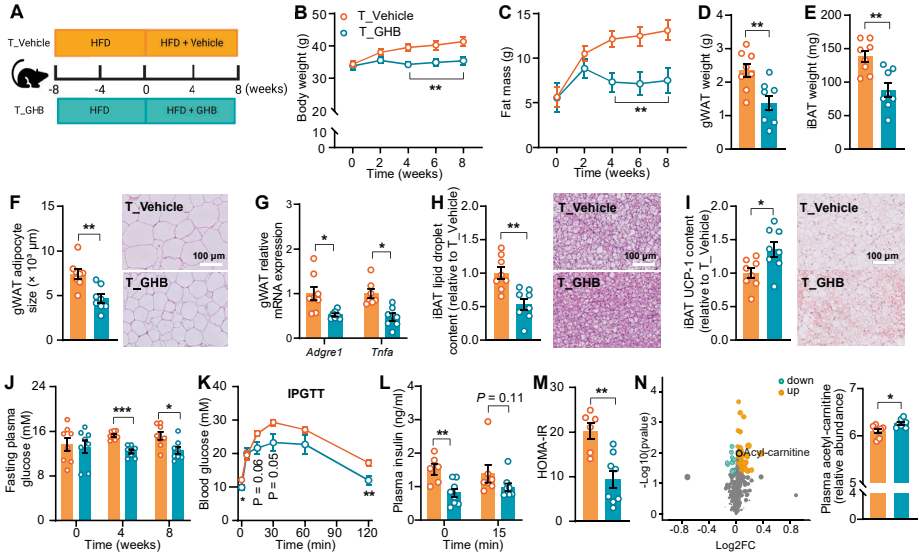

Fig. 1. Oral administration of GHB attenuates fat mass gain and improves glucose control in existing obesity. (**A**) Experimental setup. (**B**) Body weight and (**C**) fat mass were monitored throughout the experimental period. (**D-E**) At the end of the study, gonadal white adipose tissue (gWAT) and interscapular brown adipose tissue (iBAT) were collected and weighed. (**F**) White adipocyte size was assessed by hematoxylin-eosin (H&E) staining. (**G**) gWAT inflammation was assessed by quantifying proinflammatory gene expression. (**H**) Lipid droplet content and (**I**) uncoupling protein-1 (UCP-1) protein abundance in iBAT were evaluated by H&E staining and UCP-1 immunostaining, respectively. (**J**) Fasting plasma glucose levels were determined throughout the study. (**K**) At week 6, an intraperitoneal glucose tolerance test (IPGTT) was performed. (**L**) Fasting plasma insulin was measured during IPGTT. (**M**) Homeostasis model assessment of insulin resistance (HOMA-IR) was determined from fasting glucose and insulin at baseline. (**N**) At week 8, plasma metabolomics profiling was conducted, and acetyl-carnitine levels were determined by plasma metabolomics. Data are represented as means±SEM (n=8 per group). Differences were assessed using unpaired two-tailed Student's *t*-test or two-way ANOVA followed by Fisher's LSD test (**K and L**). **P*<0.05, ***P*<0.01, ****P*<0.001. *Adgre1*, adhesion G protein-coupled receptor E1; gWAT, gonadal white adipose tissue; HFD, high fat diet; iBAT, interscapular brown adipose tissue; *Tnfa*, tumor necrosis factor α.

GHB alleviates liver steatosis and inflammation, accompanied by improved retinol metabolism in existing obesity

To unravel the molecular impact of GHB treatment on peripheral tissues, untargeted metabolomics profiling of plasma from vehicle- and GHB-treated mice was performed and revealed that GHB treatment decreased 13 metabolites and increased 75 metabolites. For example, GHB treatment increased levels of acyl-carnitine (**Fig. 1N**), which is primarily generated in the liver through enhanced fatty acid (FA) oxidation [43]. In line with the body fat-lowering effect, GHB treatment reduced liver weight (**Fig. 2A**) and largely attenuated liver steatosis, as shown by reduced lipid droplets (**Fig. 2B**) and decreased TG levels (**Fig. 2C**). Untargeted metabolomic profiling of the liver identified 75 differentially regulated metabolites, including 34 downregulated

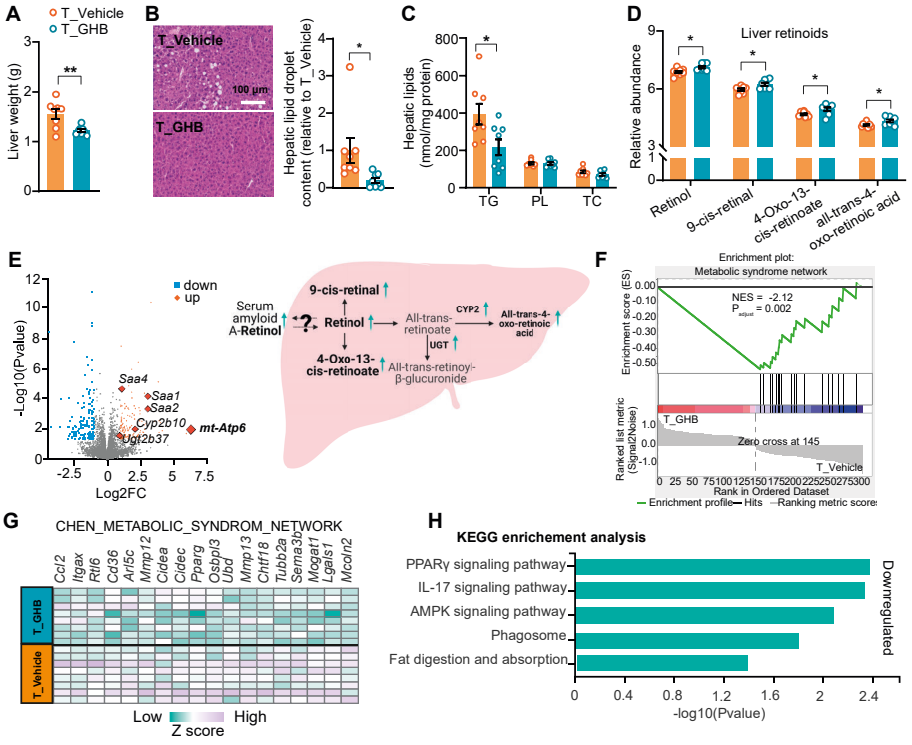

Fig. 2. GHB alleviates liver steatosis and inflammation, accompanied by improved retinol metabolism in existing obesity. (**A**) Liver weight, (**B**) liver lipid droplet content, (**C**) hepatic triglycerides (TG), phospholipids (PL) and total cholesterol (TC) were determined. (**D**) Liver retinoid levels were detected by liver metabolomics. Liver RNA sequencing was conducted, and differentially expressed genes (DEGs) were identified (**E**), and (**F**-**G**) gene set enrichment analysis (GSEA) and (**H**) KEGG pathway enrichment analysis were performed. Data are represented as means±SEM (n=8 per group). Differences were assessed using unpaired two-tailed Student's *t*-test. **P*<0.05, ***P*<0.01.

and 41 upregulated metabolites, with GHB treatment. In agreement with the hepatic lipid reduction, GHB treatment decreased hepatic fatty acids and their conjugates (**Fig. S2A**). Intriguingly, GHB increased hepatic retinoids (**Fig. S2B**), as shown by increased hepatic retinol, 9-cis-retinal, 4-oxo-13-cis-retinoate and all-trans-4-oxo-retinoic acid levels (**Fig. 2D**). Coincidingly, RNA sequencing in livers from vehicle- or GHB-treated mice revealed that GHB upregulated the hepatic expression of genes involved in retinol transport, including serum amyloid A (SAA) 1 (*Saa1*), *Saa2* and *Saa4* [45-47], and retinol metabolism, including cytochrome P450 2B10 (*Cyp2b10*) [48] and UDP-glucuronosyltransferase 2B37 (*Ugt2b37*) [49] (**Fig. 2E**).

We identified mitochondrially encoded adenosine triphosphate (ATP) synthase membrane subunit 6 (*mt-ATP6*), a gene encoding mitochondrial ATP synthase, as the most upregulated gene (**Fig. 2E**), suggesting that GHB increased mitochondrial ATP synthesis [50]. Next, we conducted gene set enrichment analysis (GSEA) and identified that GHB reduced a gene set, CHEN_METABOLIC_SYNDROM_NETWORK, which is associated with the metabolic syndrome (**Fig. 2F-G**). The Molecular Signatures Database described genes within this gene set as 'genes that form the macrophage-enriched metabolic network (MEMN) and are claimed to have a causal relationship with the metabolic syndrome traits' (**Fig. 2F-2G**) [51]. Furthermore, we showed that these downregulated genes are mainly involved in lipogenic pathway peroxisome proliferator-activated receptor γ (PPARγ) signaling and pro-inflammatory pathway interleukin 17 (IL-17) signaling, and we also observed downregulation of pathways associated with the maintenance of energy balance (i.e. AMPK signaling and fat digestion and absorption) and regulation of immune responses (i.e. phagosome) (**Fig. 2H**). Altogether, the present study indicates that in existing obesity, GHB may alleviate HFD-induced liver damage as associated with improved liver mitochondrial function.

GHB beneficially modulates the gut microbiota composition and increases succinate concentrations in the caecal content in existing obesity

As GHB is a SCFA, and the SCFAs butyrate and propionate have been shown to attenuate obesity and associated metabolic disorders by modulating the gut microbiota composition, we then performed 16S rRNA gene sequencing to evaluate the impact of GHB on the gut microbiota. GHB treatment did not affect α diversity (**Fig. 3A**), while altering β diversity (**Fig. 3B**), indicative of altered gut microbial structure. Most commensal gut microbes in the caecal content of both vehicle- and GHB-treated mice belonged to the phyla *Firmicutes* and *Bacteroidota* which, along with *Desulfobacterota* and *Actinobacteriota*, represented approximately 95% of the total microbial community (**Fig. 3C**). Moreover, *Blautia*, *Faecalibaculum* and *Colidextribacter* were the most abundant genera in both groups (**Fig. S3B**). LEfSe analysis showed that GHB treatment reduced the abundance of pro-inflammatory genera, such as *Rikenellaceae R9 gut group* (*R. R9 gut group*)[52], *Alistipes* [53], *Colidextribacter* [54] and *Escherichia Shigella* (*E. Shigella*) [55], while increasing the abundance of *Harryflintia* [56] and *Bacillus* [57], both genera with anti-inflammatory properties (**Fig. 3D**). These findings indicate that GHB beneficially modulates the gut microbiota composition. Moreover, we determined gut microbial metabolites in the cecal content, and we observed that GHB tended to increase butyrate and propionate concentrations (**Fig. 3E-F and Fig. S3B**) and significantly increased succinate concentrations (**Fig. 3G**). Thus, we demonstrate that in obesity, GHB beneficially modulates the gut microbiota composition, accompanied by increased succinate concentrations in the caecal content.

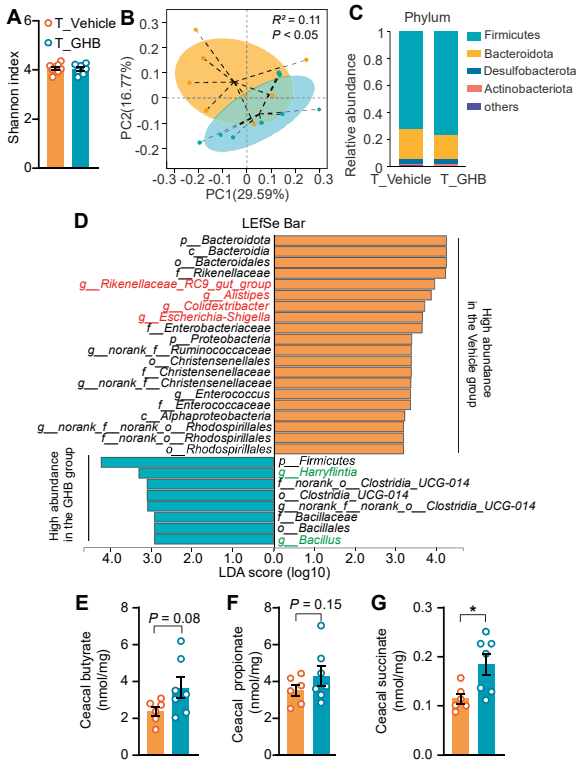

Fig. 3. GHB beneficially modulates the gut microbiota composition and increases succinate concentrations in the cecal content in existing obesity. At the end of the study, the cecal content was collected and sequenced (n=8 per group). (**A**) The Shannon index. (**B**) and Principal component analysis (PCA) were performed. (**C**) The abundance of microbial phyla. (**D**) Linear discrimination analysis (LDA) effect size analysis (LEfSe) was performed, and LDA scores calculated between groups. (**E-G**) Butyrate, and succinate levels in the caecal content were measured. Data are represented as means ± SEM (n=8 per group). Differences were assessed using unpaired two-tailed Student's t-test. *P<0.05.

GHB has no impact on body weight and glucose metabolism in developing obesity

The profound effects of GHB on body weight and glucose metabolism in obesity prompted us to also examine potential preventive effects of GHB during the development of diet-induced obesity. To this end, we fed mice a HFD while simultaneously orally administering GHB or vehicle for 8 weeks (**Fig. 4A**). GHB had no impact on food intake (**Fig. S4A**) but increased voluntary locomotor activity in the mice (**Fig. S4B**). However, GHB did neither affect body weight (**Fig. 4B**) nor body composition (**Fig. 4C** and **S4C**). Likewise, GHB had no impact on gWAT and iBAT (**Fig. 4D-G**) or plasma levels of lipids (**Fig. S4D-F**) and glucose (**Fig. 4H**). By performing plasma metabolomics analysis, we identified that GHB treatment downregulated 32 metabolites and upregulated only 6 metabolites. In developing obesity, GHB did not affect plasma acyl-carnitine levels, while GHB decreased plasma levels of the sphingosine derivative C16 sphinganine (**Fig. 4I**), which is a sphingolipid associated with NAFLD development [58].

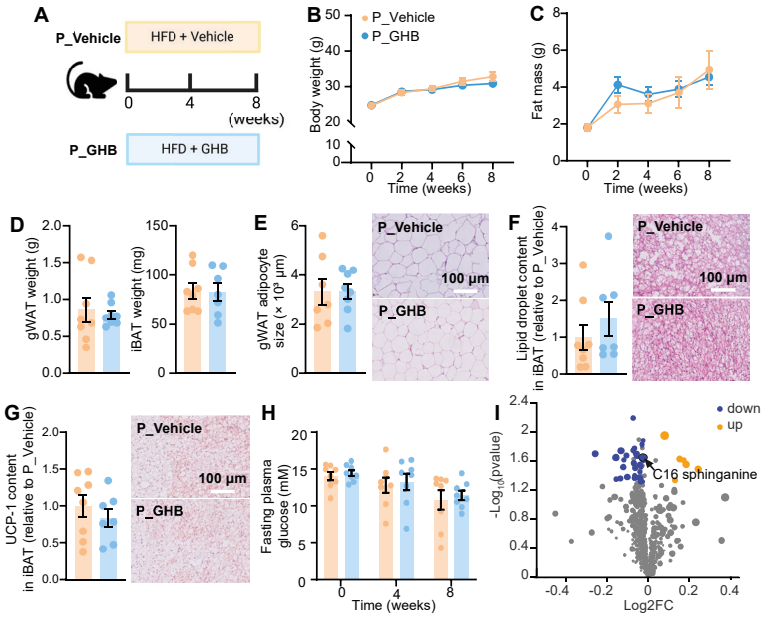

Fig. 4. GHB does not impact body weight and glucose metabolism in developing obesity. (**A**) Experimental setup. (**B**) Body weight and (**C**) body fat mass were measured throughout the experimental period. At the end of the study, (**D**) gWAT and iBAT were collected and weighed. (**E**) White adipocyte size and (**F**) iBAT lipid overload were assessed by H&E staining. (**G**) UCP-1 protein abundance was assessed in iBAT. (**H**) Fasting plasma glucose was measured throughout the study. (**I**) Plasma metabolites were determined by untargeted metabolomics. Data are represented as means±SEM (n=8 per group). Differences were assessed using unpaired two-tailed Student's *t*-test.

GHB prevents accumulation of hepatic sphingolipids, accompanied by downregulated pro-inflammatory signaling in developing obesity

While GHB treatment did not affect body weight and overall adiposity in developing obesity, GHB did decrease liver weight (**Fig. 5A**) and lowered hepatic lipid droplet content (**Fig. 5B**). GHB treatment did not significantly reduce hepatic TG, phospholipids (PL) and total cholesterol (TC) content (**Fig. 5C**), but decreased many hepatic lipids species as revealed by untargeted metabolomics profiling, including glycerophosphocholines (**Fig. S5A**), levels of which are increased in individuals with nonalcoholic steatohepatitis (NASH) [59]. Moreover, GHB increased hepatic amino acids, peptides and their analogues (**Fig. S5B**). In line with this, GHB-treated mice had increased hepatic levels of spermine (**Fig. 5D**), an amino acid metabolite with anti-oxidative and anti-inflammatory properties [60, 61]. Further analysis showed that GHB downregulated the sphingolipid signaling pathway, as deducted from reduced sphinganine and sphingosine levels in the liver (**Fig. 5D-E**). RNA sequencing in the liver also identified downregulated hepatic gene expression levels of sphingomyelin phosphodiesterase 3 (SMPD3), an enzyme

catalyzing the hydrolysis of sphingomyelin to form ceramide, with GHB treatment (**Fig. 5F**). Notably, we found cytochrome c oxidase III (*mt-Co3*), the mitochondrial gene encoding subunit IV of the respiratory complex, to be most upregulated upon GHB treatment in developing obesity (**Fig. 5F**), which suggests that GHB increases

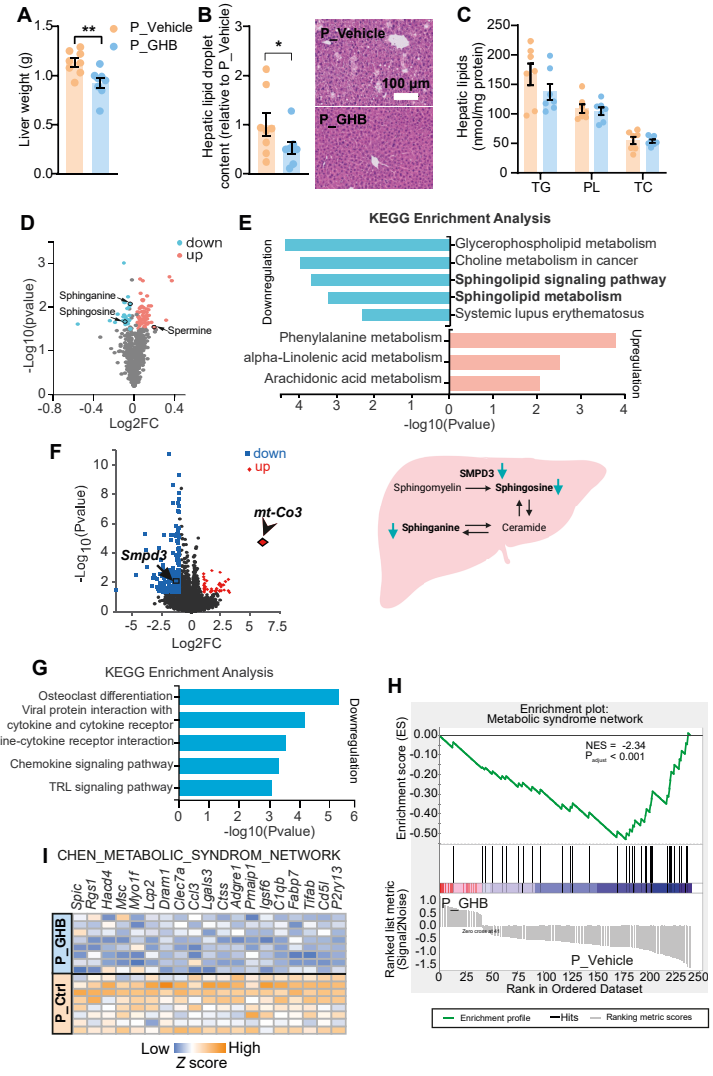

Fig. 5. GHB reduces the abundance of hepatic sphingolipids, accompanied by downregulated pro-inflammatory signaling in developing obesity. At week 8, (**A**) the liver was weighed and (**B** and **C**) hepatic lipid levels were assessed. (**D**) Hepatic metabolites were determined by untargeted metabolomics, and (**E**) KEGG pathway enrichment analysis was conducted. (**F**) Liver DEGs were identified by liver RNA sequencing and (**G**) KEGG pathway enrichment analysis and (**H-I**) GSEA were conducted. Data are represented as means ± SEM (n=8 per group). Differences were assessed using unpaired two-tailed Student's t-test. **P*<0.05, ***P*<0.01.

hepatic electron transport chain (ETC) activity. Then, focusing particularly on the downregulated genes, we identified that GHB downregulated genes enriched in immune responses, including osteoclast differentiation, viral protein interaction with cytokine and cytokine receptor, cytokine-cytokine receptor interaction, chemokine signaling and Toll-like receptor signaling (**Fig. 5G**). Consistently, GSEA analysis showed that GHB downregulated a gene set involved in macrophage-mediated metabolic syndrome development (**Fig. 5H-I**). Collectively, these data indicate that GHB, also in developing obesity, ameliorates hepatic steatosis and attenuates hepatic inflammation, accompanied by upregulation of markers of improved hepatic mitochondrial function.

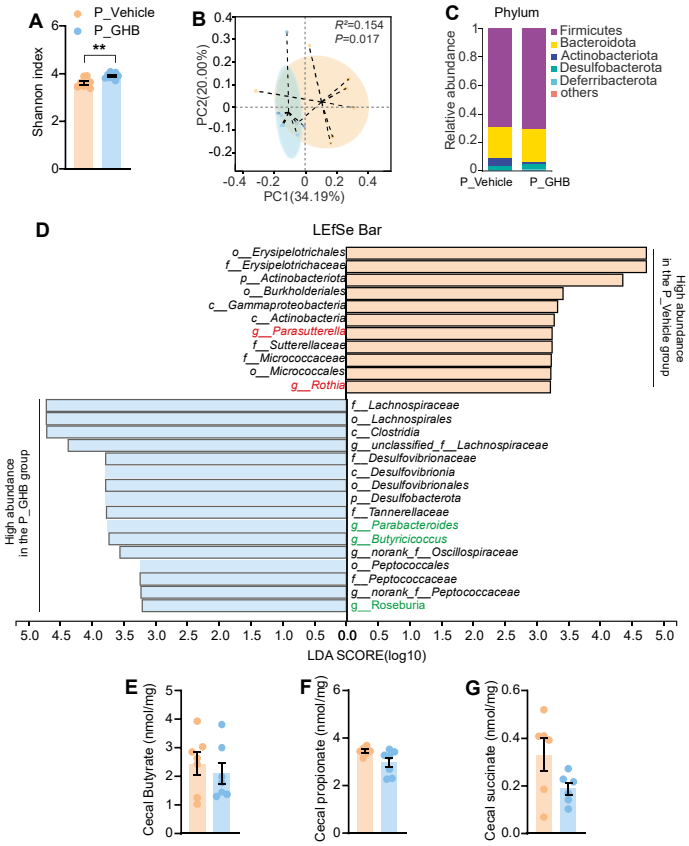

Fig. 6. GHB beneficially modulates the gut microbiota composition in developing obesity. After 8 weeks of GHB intervention, the caecal content was collected and bacterial 16S sequenced was performed (n=8 per group). (**A**) The Shannon index and (**B**) Principal component analysis (PCA) were evaluated. (**C**) The abundance of microbial phyla were detected. (**D**) LEfSe was analyzed, and LDA scores calculated between groups. (**E-G**) Butyrate, propionate and succinate levels in the caecal content were measured. Data are represented as means ± SEM (n=8 per group). Differences were assessed using unpaired two-tailed Student's t-test. $^{**}P<0.01$.

GHB beneficially modulates gut microbiota composition in developing obesity

In the setting of developing obesity, GHB increased the α diversity of the gut microbiota (**Fig. 6A**) and principal component analysis revealed a pronounced difference in β diversity (i.e. gut microbiota structure) between vehicle- and GHB-treated mice (**Fig. 6B**). Moreover, we observed that in developing obesity, *Firmicutes* and *Bacteroidota* were the most abundant phyla in both treatment groups (**Fig. S6A**), and the *Blautia* and *Faecalibaculum* (**Fig. S6B**) were abundant genera in both vehicle and GHB groups. While pro-inflammatory microbes such as *Parasutterella* and *Rothia* were more abundant in vehicle-treated mice, GHB-treated mice showed increased abundance of the SCFA-producers *Parabacteroides, Butyricicoccus* and *Roseburia* (**Fig. 6D**). However, no differences in the concentrations of microbial metabolites were detectable in cecum content (**Fig. 6E-G** and **Fig. S6B**), Taken together, these data suggest that GHB beneficially modulates the gut microbiota composition not only in existing obesity, but also in developing obesity.

DISCUSSION

Clinical studies have reported a weight loss-promoting effect of the narcolepsy drug GHB [7-9], but the underlying metabolic mechanisms remained unclear. To understand how GHB reduces body weight and thereby reveal potential therapeutic targets for obesity and its associated metabolic diseases, we set out to explore the role of GHB in body weight control under obesogenic and obese conditions. We demonstrated that GHB alleviates HFD-induced hepatic lipid accumulation and inflammation in developing and existing obesity, but only exerts weight loss-promoting and glucose-lowering effects in existing obesity. We proposed that GHB-mediated beneficial hepatic effects in both settings are associated with improved hepatic mitochondrial function. Despite the differential effects of GHB on body weight and glucose metabolism in developing and existing obesity being still unclear, a possible explanation may be the degree of hepatic lipid overload that governs hepatic mitochondrial function and systemic insulin sensitivity. In addition, we observed that GHB beneficially modulates the gut microbiota composition under both metabolic conditions, which might be also linked to the improvement of metabolic health mediated by GHB administration.

Interestingly, while GHB did not affect fat mass gain and plasma glucose levels in developing obesity, GHB did reduce liver weight and prevented HFD-induced sphingolipid accumulation and inflammation in the liver. The early onset of obesity is characterized by aberrant lipid accumulation and impaired mitochondrial function

in non-adipose tissues, particularly in the liver. In developing obesity, FA disposal through β-oxidation and TG formation is overwhelmed in non-adipose tissues. As a result, excess FAs can form lipotoxic species, such as sphingolipids, that dampen mitochondrial function and induce local and systemic inflammation. This consequently leads to the development of obesity and its associated diseases, such as NAFLD [62-65]. GHB likely improves hepatic mitochondrial function in developing obesity, as shown by a profound upregulation of hepatic *mt-Co3*, a gene encoding mitochondrial complex IV which catalyzes the last step of the mitochondrial ETC and drives oxidative phosphorylation [66]. A recent study showed that HFD feeding promotes hepatocyte lipid overload and inhibits hepatic mitochondrial complex IV, resulting in increased hepatic oxidative stress and consequently liver damage which was attenuated by restoring mitochondrial complex IV activity [67]. Therefore, upregulation of complex IV may well explain the beneficial GHB-mediated effects on the liver. Since oral GHB is mainly metabolized in the liver, and primarily in hepatocytes, through the mitochondrial TCA cycle [22], the upregulated expression of hepatic *mt-Co3* upon GHB treatment may be driven by increased TCA activity of hepatocytes. Studies have shown that mitochondrial TCA activity is essential for modulating amino acid metabolism [68]. This may well explain why levels of amino acids are increased in livers of GHB-treated mice during HFD feeding. Consistently, we found that GHB increased hepatic levels of the amino acid metabolite spermine, which is crucial for maintaining TCA cycle activity [69-72]. These findings possibly identify *mt-Co3* and spermine as potential therapeutic targets to prevent obesity and its associated metabolic disorders.

In existing obesity, GHB not only improved liver function but also reduced body weight, as explained by reduced fat mass coinciding with improved adipose tissue function and insulin sensitivity. These beneficial systemic effects are likely also linked to the improvement of mitochondrial function in hepatocytes, since GHB increased systemic levels of acyl-carnitine, a liver-derived fuel source for BAT thermogenesis [43]. Previous studies showed that upon cold exposure, WAT-derived FAs activate hepatic carnitilation to generate acyl-carnitines within hepatocyte mitochondria, and once in the circulation, acyl-carnitines can be transported to BAT while the uptake into WAT and the liver are blocked [43]. We, however, did not observe any effects of GHB on circulating NEFA and free glycerol levels in developing and existing obesity, which possibly suggests that GHB does not directly affect adipose tissue function. Instead, GHB may directly act on the liver to modulate hepatic mitochondrial function. Indeed, in existing obesity, GHB increased hepatic expression of *mt-ATP6*, a gene encoding ATP synthase, which is also known as mitochondrial complex V and responsible for the final step of oxidative phosphorylation [73, 74]. The upregulation of *mt-ATP6* may also be driven by the GHB-induced increase in TCA activity in the liver, as TCA activity

governs respiratory efficiency [75]. Obesity-driven NAFLD is associated with disturbed TCA cycle activity, impaired mitochondrial ATP synthesis and reduced mitochondrial oxidative phosphorylation activity [67, 76, 77]. In agreement with improved hepatocyte mitochondrial function, we showed a profound reduction of hepatic steatosis and inflammation in obese mice treated with GHB. The differential modulation of mitochondrial gene expression by GHB in developing and existing obesity possibly can be explained by the differences in metabolic status, the degree of hepatic lipid levels and thus hepatocyte mitochondrial dynamics. Indeed, the morphology and dynamics of mitochondria change rapidly in response to various challenges, e.g. metabolic cues, and their structure and function varies at different stages of obesity and its related diseases [78, 79].

Notably, in existing obesity, we further reported that GHB protected against HFD-induced loss of hepatic retinoids. In healthy liver, hepatic stellate cells (HSCs) are considered "quiescent", and these quiescent HSCs represent the major storage site for retinoids in the whole body, as 90-95% of retinoids in the body are stored in HSCs [44]. However, during progressive NAFLD, hepatic inflammation leads to HSC activation, resulting in loss of retinoids. The loss of retinoids can induce the production of excessive amounts of extracellular matrix proteins and consequently promote fibrogenesis in the liver [80, 81]. Accordingly, our results may indicate that GHB protects against HSC activation, which may be the consequence of increased *mt-ATP6* expression in the liver (e.g. within the hepatocytes and HSCs). In agreement, deprivation of HSCs from retinol reduces mitochondrial ATP synthesis, and restoring retinol increased energy output [81, 82]. Furthermore, previous studies showed that within the liver, the transcription level of *mt-ATP6* correlates with retinol levels [50], indicating that GHB improves mitochondrial function to alleviate liver damage. This also highlights that hepatic *mt-ATP6* is a potential therapeutic target for obesity-driven NAFLD, including liver fibrosis.

Moreover, we reported that GHB administration beneficially modulates the gut microbiota composition in developing obesity and existing obesity. In developing obesity, GHB increased the abundance of SCFA producers (i.e. acetate-producer *Parabacteroides* [83-86] and butyrate-producers *Butyricicocus* [87] and *Roseburi*a [88]). These gut microbes have been shown to exert anti-inflammatory effects and confer metabolic benefits by increasing the production of SCFAs. By serving as the primary energy source of enterocytes, SCFAs can improve the gut barrier integrity, which is associated with alleviation of systemic inflammation [83-86, 89-91]. They also can act as a signaling molecules to maintain whole-body energy balance by reducing food intake and increasing thermogenesis [92, 93]. However, we did not observe any effects on gut

microbial metabolites, including SCFAs, in the cecal content upon GHB administration under obesogenic conditions. Reasons may be that these metabolites are quickly taken up by the body of the host or that they are produced at low concentrations which hampers detection of potential elevations. Also, we did not observe any effects of GHB on food intake and adipose tissue function (i.e. WAT inflammation and BAT activation) in developing obesity. However, our group previously reported that oral butyrate supplementation exerts beneficial effects in developing obesity but not in existing obesity (Li Z, et al.; JCI Insight, in press. Based on these findings, we speculate that GHB may not directly affect the gut microbiota; instead, beneficial effects on the gut microbiota possibly resulted from direct beneficial effects of GHB on hepatocyte mitochondrial function, causing overall improvement of health.

In existing obesity, we observed increased succinate levels in the cecum content of GHB-treated mice. The succinate was likely generated by the gut microbiota instead of being a metabolic product of GHB, as we did not observe increased succinate levels in the cecum content of GHB-treated mice with developing obesity. Also, it is unclear whether GHB can even reach the cecum upon oral administration. Accordingly, *Bacillus*, a microbe that we found enriched with GHB treatment in established obesity [94, 95], is able to produce succinate [96]. Recently, gut microbiota-derived succinate and succinate-producing bacteria were reported to exert anti-obesity and glucose-lowering effects [86, 97], since succinate in the gut can upregulate the intestinal glucogenesis pathway and, as a consequence, reduce hepatic glucose production. However, GHB did not change the hepatic expression of genes involved in glucose production. This may indicates that the increased gut microbiota-derived succinate was also the consequence of improved whole-body metabolism upon GHB treatment. Despite this, further studies are need to confirm the impact of GHB treatment on intestinal gluconeogenesis and hepatic glucose production in existing obesity. Likewise, the present study cannot exclude a contribution of the GHB-mediated beneficial effects on the gut microbiota on maintaining metabolic health, and further studies are thus still needed to evaluate potential causal effects between the gut microbiota changes and metabolic health improvement.

In conclusion, GHB improves HFD-induced mitochondrial dysfunction of the liver in both developing and existing obesity in mice. Provided these effects can be translated to humans, the beneficial effects of GHB on metabolic health that is observed in patients receiving GHB as narcolepsy treatment may be explained via primary beneficial effects on the liver. We propose that mitochondrial TCA cycle activity and ETC function, spermine and retinoids are potential therapeutic targets to combat obesity-associated metabolic diseases. Collectively, our findings provide additional

evidence that mitochondria-directed therapeutic strategies hold great promise for combating a wide variety of metabolic diseases, including obesity and NAFLD.

Acknowledgments

We thank T.C.M. Streefland, A.C.M. Pronk, R.A. Lalai and S. Afkir from the Department of Internal Medicine, Division of Endocrinology, Leiden University Medical Center for the excellent technical assistance.

Author contributions

CL designed the study, carried out the research, analyzed and interpreted the results, and wrote and revised the manuscript. MZ carried out the research, interpreted the results, reviewed the manuscript. MSS, RF and GJL provided GHB and reviewed the manuscript. AV and MG performed cecum content metabolomics profiling and reviewed the manuscript. YW advised the study and reviewed the manuscript. MRB advised the study, reviewed the manuscript and obtained the funding. PCNR designed and advised the study, interpreted the results, edited, reviewed and revised the manuscript and obtained funding. MS advised the study, interpreted the results, reviewed and revised the manuscript and obtained the funding.

REFERENCES

1. Kahn, S.E., R.L. Hull, and K.M. Utzschneider, Mechanisms linking obesity to insulin resistance and type 2 diabetes. Nature, 2006. **444**(7121): p. 840-6.
2. Polyzos, S.A., J. Kountouras, and C.S. Mantzoros, Obesity and nonalcoholic fatty liver disease: From pathophysiology to therapeutics. Metabolism, 2019. **92**: p. 82-97.
3. Dombrowski, S.U., et al., Long term maintenance of weight loss with non-surgical interventions in obese adults: systematic review and meta-analyses of randomised controlled trials. BMJ, 2014. **348**: p. g2646.
4. Jastreboff, A.M., et al., Tirzepatide Once Weekly for the Treatment of Obesity. New England Journal of Medicine, 2022. **387**(3): p. 205-216.
5. Saxon, D.R., et al., Antiobesity Medication Use in 2.2 Million Adults Across Eight Large Health Care Organizations: 2009-2015. Obesity, 2019. **27**(12): p. 1975-1981.
6. Bessesen, D.H. and L.F. Van Gaal, Progress and challenges in anti-obesity pharmacotherapy. Lancet Diabetes Endocrinol, 2018. **6**(3): p. 237-248.
7. Husain, A.M., R.K. Ristanovic, and R.K. Bogan, Weight loss in narcolepsy patients treated with sodium oxybate. Sleep Med, 2009. **10**(6): p. 661-3.
8. Ponziani, V., et al., BMI changes in pediatric type 1 narcolepsy under sodium oxybate treatment. Sleep, 2021. **44**(7).
9. Noujaim, M.G., A. Mourad, and J.D. Clough, Sodium Oxybate: A Cause of Extreme Involuntary Weight Loss in a Young Lady. Case Rep Med, 2019. **2019**: p. 6537815.
10. Snead, O.C., 3rd and K.M. Gibson, Gamma-hydroxybutyric acid. N Engl J Med, 2005. **352**(26): p. 2721-32.
11. Kok, S.W., et al., Hypocretin deficiency in narcoleptic humans is associated with abdominal obesity. Obesity Research, 2003. **11**(9): p. 1147-1154.
12. Poli, F., et al., Body mass index-independent metabolic alterations in narcolepsy with cataplexy. Sleep, 2009. **32**(11): p. 1491-7.
13. Ponziani, V., et al., Growing Up with Type 1 Narcolepsy: Its Anthropometric and Endocrine Features. J Clin Sleep Med, 2016. **12**(12): p. 1649-1657.
14. Felmlee, M.A., B.L. Morse, and M.E. Morris, gamma-Hydroxybutyric Acid: Pharmacokinetics, Pharmacodynamics, and Toxicology. AAPS J, 2021. **23**(1): p. 22.
15. Maitre, M., C. Klein, and A.G. Mensah-Nyagan, Mechanisms for the Specific Properties of gamma-Hydroxybutyrate in Brain. Med Res Rev, 2016. **36**(3): p. 363-88.
16. Buchele, F., et al., Sodium Oxybate for Excessive Daytime Sleepiness and Sleep Disturbance in Parkinson Disease: A Randomized Clinical Trial. JAMA Neurol, 2018. **75**(1): p. 114-118.
17. Schep, L.J., et al., The clinical toxicology of gamma-hydroxybutyrate, gamma-butyrolactone and 1,4-butanediol. Clin Toxicol (Phila), 2012. **50**(6): p. 458-70.
18. Donjacour, C.E., et al., Glucose and fat metabolism in narcolepsy and the effect of sodium oxybate: a hyperinsulinemic-euglycemic clamp study. Sleep, 2014. **37**(4): p. 795-801.
19. Donjacour, C.E., et al., Plasma total ghrelin and leptin levels in human narcolepsy and matched healthy controls: basal concentrations and response to sodium oxybate. J Clin Sleep Med, 2013. **9**(8): p. 797-803.

20. Zhang, G.F., et al., Metabolism of gamma-hydroxybutyrate in perfused rat livers. Biochem J, 2012. **444**(2): p. 333-41.

21. Luca, G., et al., Central and peripheral metabolic changes induced by gamma-hydroxybutyrate. Sleep, 2015. **38**(2): p. 305-13.

22. Busardo, F.P. and A.W. Jones, GHB pharmacology and toxicology: acute intoxication, concentrations in blood and urine in forensic cases and treatment of the withdrawal syndrome. Curr Neuropharmacol, 2015. **13**(1): p. 47-70.

23. Dave, R.A., K.E. Follman, and M.E. Morris, gamma-Hydroxybutyric Acid (GHB) Pharmacokinetics and Pharmacodynamics: Semi-Mechanistic and Physiologically Relevant PK/PD Model. AAPS J, 2017. **19**(5): p. 1449-1460.

24. Martinez-Reyes, I. and N.S. Chandel, Mitochondrial TCA cycle metabolites control physiology and disease. Nat Commun, 2020. **11**(1): p. 102.

25. Luukkonen, P.K., et al., Distinct contributions of metabolic dysfunction and genetic risk factors in the pathogenesis of non-alcoholic fatty liver disease. J Hepatol, 2022. **76**(3): p. 526-535.

26. Wolff, G., et al., Hepatocyte-specific activity of TSC22D4 triggers progressive NAFLD by impairing mitochondrial function. Mol Metab, 2022. **60**: p. 101487.

27. Meex, R.C.R. and M.J. Watt, Hepatokines: linking nonalcoholic fatty liver disease and insulin resistance. Nat Rev Endocrinol, 2017. **13**(9): p. 509-520.

28. Strissel, K.J., et al., Adipocyte death, adipose tissue remodeling, and obesity complications. Diabetes, 2007. **56**(12): p. 2910-8.

29. Turner, N., et al., Distinct patterns of tissue-specific lipid accumulation during the induction of insulin resistance in mice by high-fat feeding. Diabetologia, 2013. **56**(7): p. 1638-48.

30. Zhao, Y., et al., Liver governs adipose remodelling via extracellular vesicles in response to lipid overload. Nat Commun, 2020. **11**(1): p. 719.

31. Canfora, E.E., J.W. Jocken, and E.E. Blaak, Short-chain fatty acids in control of body weight and insulin sensitivity. Nat Rev Endocrinol, 2015. **11**(10): p. 577-91.

32. Lu, Y., et al., Short Chain Fatty Acids Prevent High-fat-diet-induced Obesity in Mice by Regulating G Protein-coupled Receptors and Gut Microbiota. Sci Rep, 2016. **6**: p. 37589.

33. van Eenige, R., et al., RandoMice, a novel, user-friendly randomization tool in animal research. PLoS One, 2020. **15**(8): p. e0237096.

34. Bligh, E.G. and W.J. Dyer, A rapid method of total lipid extraction and purification. Can J Biochem Physiol, 1959. **37**(8): p. 911-7.

35. Chen, S., et al., fastp: an ultra-fast all-in-one FASTQ preprocessor. Bioinformatics, 2018. **34**(17): p. i884-i890.

36. Kim, D., B. Langmead, and S.L. Salzberg, HISAT: a fast spliced aligner with low memory requirements. Nat Methods, 2015. **12**(4): p. 357-60.

37. Pertea, M., et al., StringTie enables improved reconstruction of a transcriptome from RNA-seq reads. Nat Biotechnol, 2015. **33**(3): p. 290-5.

38. Li, B. and C.N. Dewey, RSEM: accurate transcript quantification from RNA-Seq data with or without a reference genome. BMC Bioinformatics, 2011. **12**: p. 323.

39. Love, M.I., W. Huber, and S. Anders, Moderated estimation of fold change and dispersion for RNA-seq data with DESeq2. Genome Biol, 2014. **15**(12): p. 550.

40. Xie, C., et al., KOBAS 2.0: a web server for annotation and identification of enriched pathways and diseases. Nucleic Acids Res, 2011. **39**(Web Server issue): p. W316-22.

41. Subramanian, A., et al., Gene set enrichment analysis: a knowledge-based approach for interpreting genome-wide expression profiles. Proc Natl Acad Sci U S A, 2005. **102**(43): p. 15545-50.

42. Kim, H.K., S. Kostidis, and Y.H. Choi, NMR Analysis of Fecal Samples. Methods Mol Biol, 2018. **1730**: p. 317-328.

43. Simcox, J., et al., Global Analysis of Plasma Lipids Identifies Liver-Derived Acylcarnitines as a Fuel Source for Brown Fat Thermogenesis. Cell Metabolism, 2017. **26**(3): p. 509-+.

44. Tsuchida, T. and S.L. Friedman, Mechanisms of hepatic stellate cell activation. Nat Rev Gastroenterol Hepatol, 2017. **14**(7): p. 397-411.

45. Derebe, M.G., et al., Serum amyloid A is a retinol binding protein that transports retinol during bacterial infection. Elife, 2014. **3**.

46. Ganal, S.C. and A.J. MacPherson, An ambulance for retinol. Elife, 2014. **3**: p. e04246.

47. Esterhazy, D. and D. Mucida, Serum amyloid A proteins take retinol for a ride. Trends Immunol, 2014. **35**(11): p. 505-6.

48. Shmarakov, I.O., Retinoid-xenobiotic interactions: the Ying and the Yang. Hepatobiliary Surg Nutr, 2015. **4**(4): p. 243-67.

49. Akimoto, Y., et al., Retinoic Acid-Induced Epidermal Transdifferentiation in Skin. Journal of Developmental Biology, 2014. **2**(3): p. 158-173.

50. Berdanier, C.D., et al., Role of vitamin A in mitochondrial gene expression. Diabetes Res Clin Pract, 2001. **54 Suppl 2**: p. S11-27.

51. Chen, Y.Q., et al., Variations in DNA elucidate molecular networks that cause disease. Nature, 2008. **452**(7186): p. 429-435.

52. Sun, L., et al., Cecal Gut Microbiota and Metabolites Might Contribute to the Severity of Acute Myocardial Ischemia by Impacting the Intestinal Permeability, Oxidative Stress, and Energy Metabolism. Frontiers in Microbiology, 2019. **10**.

53. Parker, B.J., et al., The Genus Alistipes: Gut Bacteria With Emerging Implications to Inflammation, Cancer, and Mental Health. Front Immunol, 2020. **11**: p. 906.

54. Kang, G.U., et al., Exploration of Potential Gut Microbiota-Derived Biomarkers to Predict the Success of Fecal Microbiota Transplantation in Ulcerative Colitis: A Prospective Cohort in Korea. Gut Liver, 2022. **16**(5): p. 775-785.

55. Paciello, I., et al., Intracellular Shigella remodels its LPS to dampen the innate immune recognition and evade inflammasome activation. Proc Natl Acad Sci U S A, 2013. **110**(46): p. E4345-54.

56. Li, L., et al., Crude Polysaccharide Extracted From Moringa oleifera Leaves Prevents Obesity in Association With Modulating Gut Microbiota in High-Fat Diet-Fed Mice. Front Nutr, 2022. **9**: p. 861588.

57. Paynich, M.L., S.E. Jones-Burrage, and K.L. Knight, Exopolysaccharide from Bacillus subtilis Induces Anti-Inflammatory M2 Macrophages That Prevent T Cell-Mediated Disease. Journal of Immunology, 2017. **198**(7): p. 2689-2698.

58. Montefusco, D., et al., Analysis of the Sphingolipidome in NAFLD. Methods Mol Biol, 2022. **2455**: p. 279-303.

59. Anjani, K., et al., Circulating phospholipid profiling identifies portal contribution to NASH signature in obesity. J Hepatol, 2015. **62**(4): p. 905-12.

60. Zhou, S., et al., Spermine Alleviates Acute Liver Injury by Inhibiting Liver-Resident Macrophage Pro-Inflammatory Response Through ATG5-Dependent Autophagy. Frontiers in Immunology, 2018. **9**.

61. Holbert, C.E., et al., Polyamines in cancer: integrating organismal metabolism and antitumour immunity. Nat Rev Cancer, 2022. **22**(8): p. 467-480.

62. Green, C.D., et al., Sphingolipids in metabolic disease: The good, the bad, and the unknown. Cell Metab, 2021. **33**(7): p. 1293-1306.

63. Apostolopoulou, M., et al., Specific Hepatic Sphingolipids Relate to Insulin Resistance, Oxidative Stress, and Inflammation in Nonalcoholic Steatohepatitis. Diabetes Care, 2018. **41**(6): p. 1235-1243.

64. Hammerschmidt, P., et al., CerS6-Derived Sphingolipids Interact with Mff and Promote Mitochondrial Fragmentation in Obesity. Cell, 2019. **177**(6): p. 1536-1552 e23.

65. Friedman, S.L., et al., Mechanisms of NAFLD development and therapeutic strategies. Nat Med, 2018. **24**(7): p. 908-922.

66. Li, Y.F., et al., Cytochrome c oxidase subunit IV is essential for assembly and respiratory function of the enzyme complex. Journal of Bioenergetics and Biomembranes, 2006. **38**(5-6): p. 283-291.

67. Verbeek, J., et al., Roux-en-y gastric bypass attenuates hepatic mitochondrial dysfunction in mice with non-alcoholic steatohepatitis. Gut, 2015. **64**(4): p. 673-83.

68. Ryan, D.G., et al., Disruption of the TCA cycle reveals an ATF4-dependent integration of redox and amino acid metabolism. Elife, 2021. **10**.

69. Puleston, D.J., et al., Polyamine metabolism is a central determinant of helper T cell lineage fidelity. Cell, 2021. **184**(16): p. 4186-+.

70. Puleston, D.J., et al., Polyamines and eIF5A Hypusination Modulate Mitochondrial Respiration and Macrophage Activation. Cell Metab, 2019. **30**(2): p. 352-363 e8.

71. Madeo, F., et al., Spermidine in health and disease. Science, 2018. **359**(6374).

72. Vrijsen, S., et al., ATP13A2-mediated endo-lysosomal polyamine export counters mitochondrial oxidative stress. Proc Natl Acad Sci U S A, 2020. **117**(49): p. 31198-31207.

73. Ganetzky, R.D., et al., MT-ATP6 mitochondrial disease variants: Phenotypic and biochemical features analysis in 218 published cases and cohort of 14 new cases. Hum Mutat, 2019. **40**(5): p. 499-515.

74. Ng, Y.S., et al., Pathogenic variants in MT-ATP6: A United Kingdom-based mitochondrial disease cohort study. Ann Neurol, 2019. **86**(2): p. 310-315.

75. Satapati, S., et al., Elevated TCA cycle function in the pathology of diet-induced hepatic insulin resistance and fatty liver. J Lipid Res, 2012. **53**(6): p. 1080-92.

76. Longo, M., et al., Mitochondrial dynamics and nonalcoholic fatty liver disease (NAFLD): new perspectives for a fairy-tale ending? Metabolism, 2021. **117**: p. 154708.

77. Lee, K., et al., Hepatic Mitochondrial Defects in a Nonalcoholic Fatty Liver Disease Mouse Model Are Associated with Increased Degradation of Oxidative Phosphorylation Subunits. Mol Cell Proteomics, 2018. **17**(12): p. 2371-2386.

78. Fromenty, B. and M. Roden, Mitochondrial alterations in fatty liver diseases. J Hepatol, 2022.

79. Wai, T. and T. Langer, Mitochondrial Dynamics and Metabolic Regulation. Trends Endocrinol Metab, 2016. **27**(2): p. 105-117.

80. Okuno, M., et al., Retinoids exacerbate rat liver fibrosis by inducing the activation of latent TGF-beta in liver stellate cells. Hepatology, 1997. **26**(4): p. 913-21.

81. Trivedi, P., S. Wang, and S.L. Friedman, The Power of Plasticity-Metabolic Regulation of Hepatic Stellate Cells. Cell Metab, 2021. **33**(2): p. 242-257.

82. Chiu, H.J., D.A. Fischman, and U. Hammerling, Vitamin A depletion causes oxidative stress, mitochondrial dysfunction, and PARP-1-dependent energy deprivation. FASEB J, 2008. **22**(11): p. 3878-87.

83. Ezeji, J.C., et al., Parabacteroides distasonis: intriguing aerotolerant gut anaerobe with emerging antimicrobial resistance and pathogenic and probiotic roles in human health. Gut Microbes, 2021. **13**(1): p. 1922241.

84. Lei, Y.Y., et al., Parabacteroides produces acetate to alleviate heparanase-exacerbated acute pancreatitis through reducing neutrophil infiltration. Microbiome, 2021. **9**(1).

85. Wu, T.R., et al., Gut commensal Parabacteroides goldsteinii plays a predominant role in the anti-obesity effects of polysaccharides isolated from Hirsutella sinensis. Gut, 2019. **68**(2): p. 248-262.

86. Wang, K., et al., Parabacteroides distasonis Alleviates Obesity and Metabolic Dysfunctions via Production of Succinate and Secondary Bile Acids. Cell Rep, 2019. **26**(1): p. 222-235 e5.

87. Trachsel, J., S. Humphrey, and H.K. Allen, Butyricicoccus porcorum sp. nov., a butyrate-producing bacterium from swine intestinal tract. Int J Syst Evol Microbiol, 2018. **68**(5): p. 1737-1742.

88. Kasahara, K., et al., Interactions between Roseburia intestinalis and diet modulate atherogenesis in a murine model. Nature Microbiology, 2018. **3**(12): p. 1461-1471.

89. Seo, B., et al., Roseburia spp. Abundance Associates with Alcohol Consumption in Humans and Its Administration Ameliorates Alcoholic Fatty Liver in Mice. Cell Host Microbe, 2020. **27**(1): p. 25-40 e6.

90. Eeckhaut, V., et al., Butyricicoccus pullicaecorum in inflammatory bowel disease. Gut, 2013. **62**(12): p. 1745-1752.

91. Rodriguez, J., et al., Discovery of the gut microbial signature driving the efficacy of prebiotic intervention in obese patients. Gut, 2020. **69**(11): p. 1975-1987.

92. Li, Z., et al., Butyrate reduces appetite and activates brown adipose tissue via the gut-brain neural circuit. Gut, 2018. **67**(7): p. 1269-1279.

93. Gao, Z., et al., Butyrate improves insulin sensitivity and increases energy expenditure in mice. Diabetes, 2009. **58**(7): p. 1509-17.

94. Huang, J., et al., Enterococcus faecium R0026 Combined with Bacillus subtilis R0179 Prevent Obesity-Associated Hyperlipidemia and Modulate Gut Microbiota in C57BL/6 Mice. J Microbiol Biotechnol, 2021. **31**(2): p. 181-188.

95. Cao, G.T., et al., Bacillus licheniformis, a potential probiotic, inhibits obesity by modulating colonic microflora in C57BL/6J mice model. J Appl Microbiol, 2019. **127**(3): p. 880-888.

96. Hederstedt, L., Succinate:quinone oxidoreductase in the bacteria Paracoccus denitrificans and Bacillus subtilis. Biochim Biophys Acta, 2002. **1553**(1-2): p. 74-83.

97. De Vadder, F., et al., Microbiota-Produced Succinate Improves Glucose Homeostasis via Intestinal Gluconeogenesis. Cell Metab, 2016. **24**(1): p. 151-7.

SUPPLEMENT

Expanded methods

Measurement of body weight and body composition

Body weight was measured weekly with a scale, and body composition of conscious mice was measured every 2 weeks using an EchoMRI-100 analyzer (EchoMRI, Houston, TX, USA).

Locomotor activity measurement

After 2 weeks of GHB treatment, mice (n=8 per group) were single housed in fully automated metabolic cages (Promethion line, Sable Systems International, Las Vegas, NV, USA). These mice were first acclimatized to the system for 48 hours, then further monitored for another 48 hours (2 light/dark cycles), during which the locomotor activity was continuously measured.

Plasma parameters

Every 4 weeks, after 4-hour fasting, tail vein blood (n=8 per group) was collected into paraoxon-coated glass capillaries. Plasma was collected and measured for glucose, triglycerides (TG), non-esterified fatty acids (NEFAs) and free glycerol using commercial kits (Roche Diagnostics, Mannheim, Germany).

Glucose tolerance test

In the first experiment, at week 6, an intraperitoneal glucose tolerance test (IPGTT) was conducted with an injection of D-glucose (2 g/kg body weight) after 4-hour fasting (n=8 per group). Plasma glucose was measured before (0 min), and 15, 30, 60 and 120 min after D-glucose injection with a OneTouch Ultra glucometer (AccuCheck Sensor, Roche Diagnostics, Almere, The Netherlands) in a drop of tail vein blood. Extra blood was collected at t=0 and 15 min, spun down, and the serum samples were stored at -20℃ for glucose measurement (t=0) using a commercial enzymatic kit and insulin measurement (t=1 and 15 min) using the Ultra Sensitive Mouse Insulin ELISA kit (Crystal Chem, Zaandam, The Netherlands).

Adipose tissue histology

At the end of both experiments, various adipose tissue depots were collected. Formalin-fixed paraffin-embedded interscapular brown adipose tissue (iBAT) and gonadal white adipose tissue (gWAT) sections (5 μm thickness) were prepared for hematoxylin-eosin (H&E) staining. In addition, iBAT was processed for uncoupling protein-1 (UCP-1) staining. Using Image J software (version 1.52a; National Institutes of Health, Bethesda,

Maryland), the areas occupied by intracellular lipid vacuoles and UCP-1, as well as the size of adipocytes of gWAT were assessed.

Liver histology and lipid measurements

Formalin-fixed paraffin-embedded liver samples (n=8 per group) were stained with H&E. The unstained areas occupied by intracellular lipid vacuoles were quantified using Image J software. Hepatic lipids were extracted from frozen liver samples (n=8 per group) using a modified protocol from Bligh and Dyer [1]. Commercial kits were used for the measurement of hepatic TG, total cholesterol (TC), phospholipids (PL) and protein (Pierce, Thermo Fisher Scientific, Waltham, MA, USA). Hepatic lipids were expressed as nmol lipid per mg protein.

RNA sequencing analysis

Total RNA was extracted from frozen livers (n=8 per group), and RNA sequencing was performed by BGI Genomic Services (Hong Kong) and analyzed by Majorbio BioTech Co., Ltd (Shanghai, China). The Illumina HiSeq 2500 platform was used to construct RNA libraries and generate 2×150 bp long paired-end reads (Illumina, San Diego, CA, USA). The raw data end reads were trimmed and quality controlled by FASTQ with default parameters (https://github.com/OpenGene/fastp) [2], and the clean reads were separately aligned to the reference genome (GRCm38) with orientation mode (5′ to 3′ orientation) using the HISAT2 software (http://ccb.jhu.edu/software/hisat2/index.shtml) [3]. The mapped reads of each sample were assembled by StringTie in a reference-based approach (https://ccb.jhu.edu/software/stringtie/) [4]. To identify differentially expressed genes (DEGs) between the vehicle and GHB groups, the expression levels of each gene were calculated according to the transcripts per million reads (TPM) method. RSEM (http://deweylab.biostat.wisc.edu/rsem/) was used to quantify gene abundance [5]. Analysis of differential gene expression was performed using DESeq2 [6], and DEGs are defined as fold changes >2 and $P<0.05$. Volcano plots were generated using the EnhancedVolcano feature (https://github.com/kevinblighe/EnhancedVolcano). Kyoto Encyclopedia of Genes and Genomes (KEGG) pathway enrichment analysis was carried out by KOBAS (http://kobas.cbi.pku.edu.cn/home.do) [7]. Gene Set Enrichment analysis (GSEA) was also conducted to identify gene sets that share common biological function and significantly regulated gene sets were annotated based on the Molecular Signatures Database [8].

Quantitative reverse transcriptase-PCR

Using Tripure RNA isolation reagent (Roche, Mijdrecht, The Netherlands), total RNA was extracted from snap-frozen tissues (n=8 per group). Using Moloney Murine Leukemia Virus Reverse Transcriptase (Promega, Leiden, The Netherlands),

complementary DNA for quantitative reverse transcriptase-PCR was generated by reverse transcription of total RNA. Then, mRNA expression was normalized to *b-actin* and *Rplp0* mRNA levels and expressed as fold change compared with the Vehicle group. Primer sequences are listed in the **Supporting table 1.**

Plasma and liver untargeted metabolomics analysis

Lipids were extracted from plasma (~50 µL; n=8 per group) using 400 µL methanol: acetonitrile (1:1; v/v) solution. The mixture was then sonicated at 40 kHz for 30 min at 4℃ and placed at -20℃ for 30 min to precipitate proteins. After centrifugation at 13,000 rpm at 4℃ for 15 min, the supernatant was carefully transferred into new microtubes and dried under a gentle stream of nitrogen. Then, samples were reconstituted in 100 µL loading solution of acetonitrile: water (1:1; v/v) by brief sonication in a 5℃ water bath. The extracted metabolites were spun for 15 min at 13,000 g at 4℃ and the supernatant was transferred to new microtubes for LC-MS/MS analysis. Liver samples (~50 mg) were weighed, and the metabolites were extracted using 400 µL methanol:water (4:1, v/v) solution with 0.02 mg/mL L-2-chorophenylalanin as internal standard. The mixture was allowed to settle at -10℃ and treated in the high throughput tissue crusher Wonbio-96c at 50 Hz for 6 min followed by ultrasound at 40 kHz for 30 min at 5℃. The samples were placed at -20℃ for 30 min to precipitate proteins. After centrifugation at 13,000 at 4℃ for 15 min, the supernatant was carefully transferred to sample vials for LC-MS/MS analysis. As a part of the system conditioning and quality control process, a pooled quality control (QC) was prepared by mixing equal volumes of all samples. The QC samples were disposed and tested in the same manner as the samples.

The UHPLC-Q Exactive system was used for LC-MS analysis. Samples (~2 µL) were separated by HSS T3 column and then detected by mass spectrometry. The mobile phases contained 0.1% formic acid in water : acetonitrile (95:5, v/v) (solvent A) and 0.1% formic acid in acetonitrile : isopropanol : water (47.5:47.5:5, v/v) (solvent B). The solvent gradient changed according to the following conditions: 0-0.1 min, 0% B to 5% B; 0.1-2 min, 5% B to 25% B; 2- 9 min, 25% B to 100% B; 9-13 min, 100% B to 100% B; 13-13.1 min, 100% B to 0% B ; 13.1-16 min, 0% B to 0% B for equilibrating the systems. The injection volume of samples was 2 µL, and the sample flow rate was set to 0.4 mL/min. The column temperature was maintained at 40℃. The mass spectrometric detection were then conducted using a UHPLC-Q Exactive Mass Spectrometer equipped with an electrospray ionization (ESI) source which can handle metabolites in either a positive or a negative ion mode. The optimal conditions of the detection were set as following: heater temperature, 400℃; capillary temperature, 320℃; sheath gas flow rate, 40 arb; aux gas flow rate, 10 arb; ion-spray voltage floating (ISVF), -2800 V in negative mode and 3500 V in positive mode, respectively; Normalized collision energy, 20-40-60 V rolling

for MS/MS. Full MS resolution was 70,000, and MS/MS resolution was 17,500. Data was collected using the Data Dependent Acquisition (DDA) mode. The detection was carried out over a mass range of 70-1050 m/z. After completing the mass spectrometry detection, the raw data was proceeded by Progenesis QI software (Waters Corporation, Milford, USA), and a three-dimensional data matrix in CSV format was acquired. In order to reduce the errors caused by sample preparation and instrument instability, the response intensity of the sample mass spectrum peaks was normalized by the sum normalization method, and the normalized data matrix was obtained. At the same time, variables with relative standard deviation (RSD) > 30% of quality control (QC) samples were removed, and log10 logarithmization was performed to obtain the final data matrix for subsequent analysis.

The metabolites were searched and identified, and the main database was the HMDB (http://www.hmdb.ca/). Orthogonal least partial squares discriminant analysis (OPLS-DA) was performed using the R package ropls (Version 1.6.2), and 7-cycle interactive validation was used to evaluate the stability of the model. In addition, Student's *t*-test and fold difference analysis were performed. The selection of significantly different metabolites was determined based on the Variable importance in the projection (VIP) obtained by the OPLS-DA model and the *P*-value of Student's *t*-test. The metabolites with VIP>1, $P<0.05$ were defined as significantly different metabolites. Differential metabolites among two groups were summarized, and mapped into their biochemical pathways through metabolic enrichment and pathway analysis based on database search (KEGG, http://www. genome.jp/kegg/). These metabolites can be classified according to the pathways they are involved in or the functions they perform. Enrichment analysis was conducted using Python packages (https://docs.scipy.org/doc/scipy/).

Gut microbial metabolites measurement

The method for the NMR analysis of cecum content samples was adapted from the protocol developed for human fecal samples with a few changes [9]. The mass of each cecal content sample (~50 mg) was carefully weighed prior to the sample preparation. To each sample tube, 50 µL of 0.5 mm zirconium oxide beads (Next Advance, Inc. USA, New York), ceramic beads and 300 µL of pH 7.4 potassium phosphate buffer (0.15 M) containing 0.2 mM NaN_3 were added. Then, these tubes were subjected to bead beating for 30 seconds. The tubes were subsequently centrifuged at 18,000 g at 4℃ for 15 minutes. 250 µL of supernatant was transferred to new 1.5 mL Eppendorf tubes. These tubes were centrifuged at 18,000 g at 4℃ for 1 hour. 225 µL of supernatant was added to 25 µL of 100% D_2O containing 4 mM TSP-d4, and 6 mM dimethylsulfone. A

customized Gilson 215 liquid handler was used to transfer the samples to a 3.0 mm Bruker NMR tube rack.

^{1}H NMR data were collected using a Bruker 600 MHz Avance Neo/IVDr spectrometer equipped with a 5 mm TCI cryogenic probe head and a z-gradient system. A Bruker SampleJet sample changer was used for sample insertion and removal. All experiments were recorded at 300 K. A standard sample 99.8% methanol-d4 was used for temperature calibration before each batch of measurements [10]. One-dimensional (1D) ^{1}H NMR spectra were recorded using the first increment of a NOESY pulse sequence [11] with presaturation (γB1=50 Hz) during a relaxation delay of 4 s and a mixing time of 10 ms for efficient water suppression [12]. Initial shimming was performed using the TopShim tool on a random mix of urine samples from the study, and subsequently the axial shims were optimized automatically before every measurement. Duration of 90° pulses were automatically calibrated for each individual sample using a homonuclear-gated mutation experiment on the locked and shimmed samples after automatic tuning and matching of the probe head [13]. 16 scans of 65,536 points covering 12,335 Hz were recorded. The Free Induction Decay of the 1D experiment was zero-filled to 65,536 complex points prior to Fourier transformation. An exponential window function was applied with a line-broadening factor of 0.3 Hz. The spectra were automatically phase and baseline corrected and automatically referenced to an internal standard (TSP=0.0 ppm). Metabolites were quantified in a select number of spectra using the Chenomx NMR Suite (version 8.6), and by fitting the remaining spectra automatically in the KIMBLE environment [14]. The areas were converted to concentrations using the dimethylsulfone internal standard.

16S rRNA gene sequencing

After 8 weeks of GHB intervention, cecal contents (n=8 per group) were collected, and genomic bacterial DNA was isolated with the fast DNA stool mini kit (QIAamp, Manheim, Germany) following the manufacturer's instructions. Then, these DNA samples were used for 16S rRNA sequencing at BGI Genomics and analyzed by Majorbio BioTech Co., Ltd. Briefly, microbial DNA was amplified using a set of barcoded dual-index primers encoding the V3-V4 region of the 16S rRNA gene. A high-sensitive DNA analysis kit (Agilent, San Diego, CA, USA) was used to confirm the size of the amplicon library (~399 bp). The pooled amplicon library was then sequenced on the Illumina MiSeq platform using the 500 cycle MiSeq V2 Reagent kit (Illumina, San Diego, CA, USA) according to the manufacturer's instructions. The "Preparing Libraries for Sequencing on the MiSeq" protocol was used to prepare libraries with a final load concentration of 5.5 p.m., spiked with 15% PhiX to create diversity within the run. FASTQ files are generated when the 2x250 bp sequencing completes. Following

sequencing, microbiome bioinformatics were run using QIIME 2 2020.2. Briefly, non-singleton amplicon sequence variants (ASVs, 100% operational taxonomic units; OTUs) were generated from raw sequences after trimming with the cut-adapt plugin and denoising with the Dada2 plugin. Taxonomy was then assigned to ASVs using the classify-sklearn alignment algorithm against the GreenGenes database of 99% OTUs reference sequences. The α diversity (Shannon) and β diversity were calculated using the diversity plugin. Linear discriminant analysis (LDA) effect size (LEfSe) was computed to identify significantly different microbes in abundance between groups at different taxonomic levels.

Supporting table 1. List of polymerase chain reaction primer sequences used in mRNA expression analysis.

Gene	**Forward primer (5'-3')**	**Reverse Primer (5'-3')**
Acta2	CCTGACGGGCAGGTGATC	ATGAAAGATGGCTGGAAGAGAGTCT
Actb	AACCGTGAAAAGATGACCCAGAT	CACAGCCTGGATGGCTACGTA
Adgre1	CTTTGGCTATGGGCTTCCAGTC	GCAAGGAGGACAGAGTTTATCGTG
Rplp0	GGACCCGAGAAGACCTCCTT	GCACATCACTCAGAATTTCAATGG
Tnf	AGCCCACGTCGTAGCAAACCAC	TCGGGGCAGCCTTGTCCCTT

Acta2, actin α 2; *Actb*, β-actin *Adgre1*, adhesion G protein-coupled receptor E1; *Rplp0,* ribosomal protein lateral stalk subunit p0; *Tnf*, tumor necrosis factor α.

REFERENCES

1. Bligh, E.G. and W.J. Dyer, *A rapid method of total lipid extraction and purification.* Can J Biochem Physiol, 1959. **37**(8): p. 911-7.
2. Chen, S., et al., *fastp: an ultra-fast all-in-one FASTQ preprocessor.* Bioinformatics, 2018. **34**(17): p. i884-i890.
3. Kim, D., B. Langmead, and S.L. Salzberg, *HISAT: a fast spliced aligner with low memory requirements.* Nat Methods, 2015. **12**(4): p. 357-60.
4. Pertea, M., et al., *StringTie enables improved reconstruction of a transcriptome from RNA-seq reads.* Nat Biotechnol, 2015. **33**(3): p. 290-5.
5. Li, B. and C.N. Dewey, *RSEM: accurate transcript quantification from RNA-Seq data with or without a reference genome.* BMC Bioinformatics, 2011. **12**: p. 323.
6. Love, M.I., W. Huber, and S. Anders, *Moderated estimation of fold change and dispersion for RNA-seq data with DESeq2.* Genome Biol, 2014. **15**(12): p. 550.
7. Xie, C., et al., *KOBAS 2.0: a web server for annotation and identification of enriched pathways and diseases.* Nucleic Acids Res, 2011. **39**(Web Server issue): p. W316-22.
8. Subramanian, A., et al., *Gene set enrichment analysis: a knowledge-based approach for interpreting genome-wide expression profiles.* Proc Natl Acad Sci U S A, 2005. **102**(43): p. 15545-50.
9. Kim, H.K., S. Kostidis, and Y.H. Choi, *NMR Analysis of Fecal Samples.* Methods Mol Biol, 2018. **1730**: p. 317-328.
10. Findeisen, M., T. Brand, and S. Berger, *A 1H-NMR thermometer suitable for cryoprobes.* Magn Reson Chem, 2007. **45**(2): p. 175-8.
11. Kumar, A., R.R. Ernst, and K. Wuthrich, *A two-dimensional nuclear Overhauser enhancement (2D NOE) experiment for the elucidation of complete proton-proton cross-relaxation networks in biological macromolecules.* Biochem Biophys Res Commun, 1980. **95**(1): p. 1-6.
12. Vilen, E.M., M. Klinger, and C. Sandstrom, *Application of diffusion-edited NMR spectroscopy for selective suppression of water signal in the determination of monomer composition in alginates.* Magn Reson Chem, 2011. **49**(9): p. 584-91.
13. Wu, P.S. and G. Otting, *Rapid pulse length determination in high-resolution NMR.* J Magn Reson, 2005. **176**(1): p. 115-9.
14. Verhoeven, A., M. Giera, and O.A. Mayboroda, *KIMBLE: A versatile visual NMR metabolomics workbench in KNIME.* Anal Chim Acta, 2018. **1044**: p. 66-76.

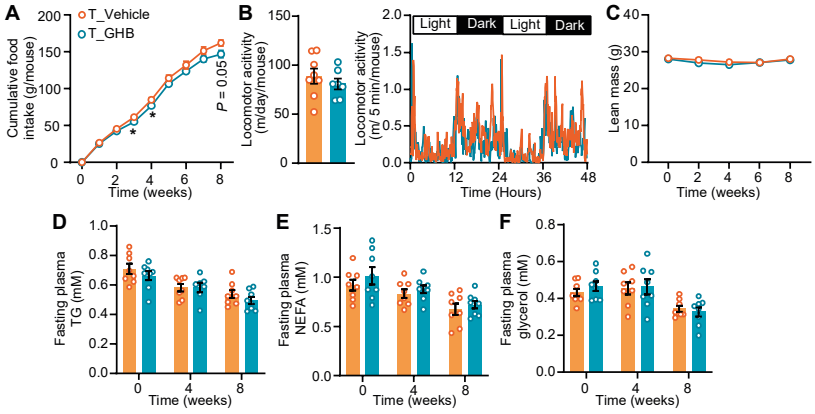

Fig. S1. GHB has no impact on food intake, locomotor activity, body lean mass and fasting plasma lipids in existing obesity. (**A**) Food intake, (**C**) body lean mass, (**D**) fasting plasma levels of triglyceride (TG), (**E**) non-esterified fatty acids (NEFA) and (**F**) free glycerol were monitored throughout the experimental period. (**B**) At week 2, locomotor activity was measured. Data are represented as means ± SEM (n=7-8 per group). Differences were assessed using unpaired two-tailed Student's *t*-test. **P*<0.05.

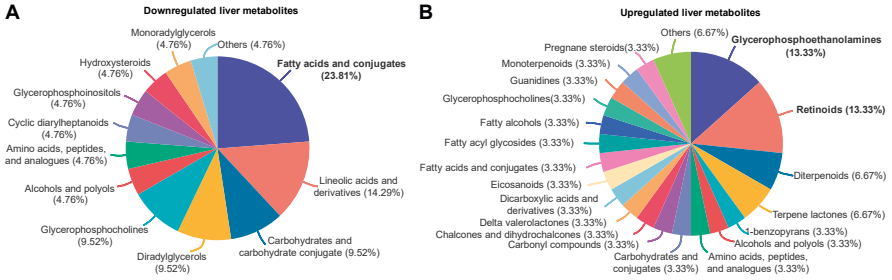

Fig. S2. GHB increases hepatic retinoids in existing obesity. After 8 weeks of GHB treatment, liver samples (n=8 per group) were collected and used for untargeted metabolomics. Differentially modulated hepatic metabolites were detected and analyzed, and the percentage of each metabolite species is depicted as pie chart.

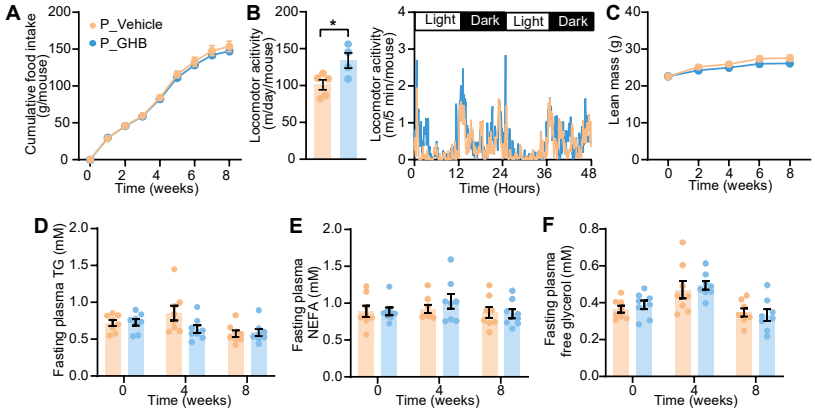

Fig. S4. GHB increases locomotor activity in developing obesity. (**A**) Food intake, (**C**) body lean mass, (**D**) fasting plasma levels of triglyceride (TG), (**E**) non-esterified fatty acids (NEFA) and (**F**) free glycerol were monitored throughout the experimental period. (**B**) At week 2, locomotor activity was measured. Data are represented as means±SEM (n=7-8 per group). Differences were assessed using unpaired two-tailed Student's *t*-test. **P*<0.05.

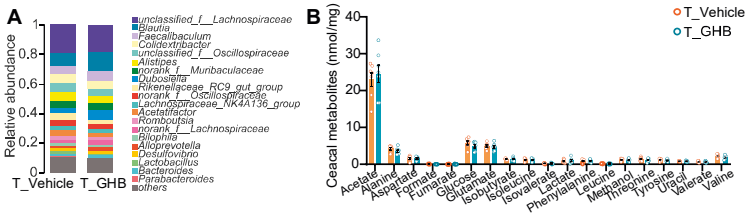

Fig. S3. GHB has no impact on gut microbial metabolites in existing obesity. At the end of the study, the cecal content was collected and the bacterial DNA sequenced (n=8 per group). (**A**) The abundance of microbial genera was evaluated. (**B**) Gut microbial metabolites were determined by performing metabolomics using cecum content samples from vehicle- and GHB-treated mice. Data are represented as means±SEM (n=8 per group).

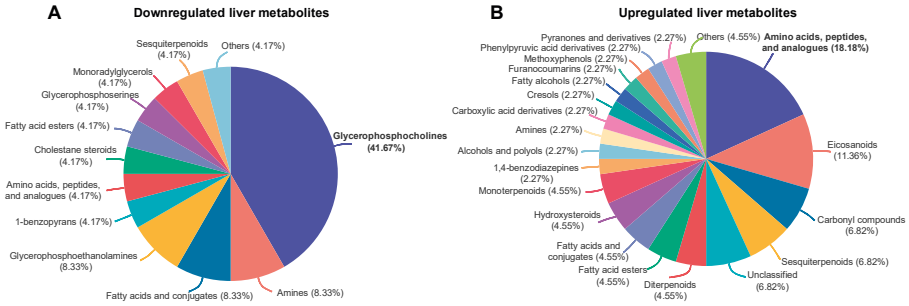

Fig. S5. GHB decreases glycerophosphocholine and increases hepatic amino acids, peptides and analogues in developing obesity. After 8 weeks of GHB interventions, liver samples (n=8 per group) were collected and used for untargeted metabolomics. Differentially modulated hepatic metabolites were detected and analyzed, and the percentage of each metabolite species was depicted as pie chart.

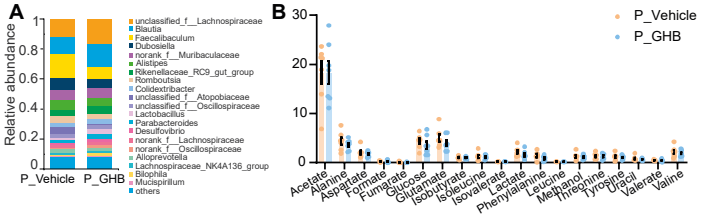

Fig. S6. GHB has no impact on gut microbial metabolites in developing obesity. At the end of the study, the cecal content was collected and the bacterial DNA sequenced (n=8 per group). (**A**) The abundance of microbial genera was evaluated. (**B**) Gut microbial metabolites were determined by performing metabolomics using cecum content samples from vehicle- and GHB-treated mice. Data are represented as means±SEM (n=8 per group).

Table S1 Plasma Metabolomics

ID	Metab ID	Formula	Metabolite	Significant	Regulate
neg_74	metab_20264	C10H19NO3	Capryloylglycine	yes	up
neg_105	metab_20295	C18H28O2	9,12-Octadecadiynoic Acid	yes	up
neg_137	metab_20327	C14H28O3	2-Hydroxymyristic Acid	yes	up
neg_327	metab_20513	C12H22O6	Phaseolic acid	yes	up
neg_575	metab_20756	C20H26O5	3-Epinobilin	yes	up
neg_702	metab_20880	C21H32O5	3a,11b,21-Trihydroxy-20-oxo-5b-pregnan-18-al	yes	up
neg_1157	metab_21327	C18H30O3	9(S)-HOTrE	yes	up
neg_2485	metab_22557	C14H24O8	Valproic acid glucuronide	yes	up
neg_3165	metab_23160	C12H18O4	3,4-Methylenesebacic acid	yes	up
neg_4216	metab_24124	C14H26O5	3-Hydroxytetradecanedioic acid	yes	up
neg_6186	metab_25932	C23H46NO8P	GPEtn(16:0/2:0)	yes	up
neg_8216	metab_27918	C17H34O3	12-hydroxyheptadecanoic acid	yes	up
neg_9559	metab_29168	C21H36O9	Glucosyl (2E,6E,10x)-10,11-dihydroxy-2,6-farnesadienoate	yes	up
neg_9806	metab_29396	C16H24O4	Methyl (3b,11x)-3-Hydroxy-8-oxo-6-eremophilen-12-oate	yes	up
neg_12049	metab_31443	C12H20O4	Traumatic Acid	yes	up
neg_12757	metab_32084	C26H30O13	6-{2-[3-(2,4-dihydroxyphenyl)propanoyl]-6-[(3,3-dimethyloxiran-2-yl)methyl]-3,5-dihydroxyphenoxy}-3,4,5-trihydroxyoxane-2-carboxylic acid	yes	up
neg_12992	metab_32302	C9H12O6S	(4-ethyl-2-hydroxy-6-methoxyphenyl) oxidanesulfonic acid	yes	up
neg_3258	metab_23240	C15H16O5	Ursinic acid	yes	down
neg_4585	metab_24459	C11H16O6S	[4-(3-hydroxybutyl)-2-methoxyphenyl] oxidanesulfonic acid	yes	down
neg_6423	metab_26159	C28H54NO7P	LysoPC(20:2(11Z,14Z))	yes	down
neg_8199	metab_27901	C28H52NO7P	LysoPC(20:3(5Z,8Z,11Z))	yes	down
neg_8543	metab_28219	C27H44O7	Crustecdysone	yes	down
neg_10903	metab_30393	C24H40O6	1b-Hydroxycholic acid	yes	down
neg_12065	metab_31458	C10H9NO3	5-Phenyl-1,3-oxazinane-2,4-dione	yes	down
pos_26	metab_25	C8H15NO3	Hexanoylglycine	yes	up
pos_49	metab_48	C15H24O2	Capsidiol	yes	up
pos_78	metab_77	C18H34O2	Petroselinic acid	yes	up
pos_100	metab_99	C13H22O2	Propyl 2,4-decadienoate	yes	up
pos_101	metab_100	C10H20O3	3-Hydroxycapric acid	yes	up
pos_102	metab_101	C20H28O4	5,6-epoxy,18R-HEPE	yes	up
pos_150	metab_149	C15H24O2	Dihydro-alpha-santalic acid	yes	up
pos_286	metab_285	C16H32O3	16-Hydroxy hexadecanoic acid	yes	up

Table S1 Plasma Metabolomics (continued)

ID	Metab ID	Formula	Metabolite	Significant	Regulate
pos_508	metab_504	C20H28O5	Bakkenolide C	yes	up
pos_547	metab_543	C14H24O2	8-Tetradecynoic acid	yes	up
pos_713	metab_709	C24H50NO6P	PC(P-16:0/0:0)	yes	up
pos_726	metab_722	C17H34O3	Avocadene	yes	up
pos_747	metab_742	C16H30O2	11Z-hexadecenoic acid	yes	up
pos_773	metab_768	C20H30O3	8(S)-HEPE	yes	up
pos_794	metab_788	C20H28O3	Phytocassane E	yes	up
pos_801	metab_795	C11H18O2	(2E,6Z)-2,6-Nonadien-1-Yl acetate	yes	up
pos_814	metab_807	C15H26O3	8-Hydroxy-4(6)-lactarene-5,14-diol	yes	up
pos_844	metab_837	C13H22O3	4,5-Dihydrovomifoliol	yes	up
pos_1714	metab_1700	C10H19NO4	O-propanoyl-carnitine	yes	up
pos_1898	metab_1884	C9H16O2	4-hydroxy Nonenal	yes	up
pos_2066	metab_2048	C15H24O3	Zedoarondiol	yes	up
pos_2090	metab_2072	C20H30O4	Prostaglandin-c2	yes	up
pos_2315	metab_2295	C20H20O3	3-(5-hydroxy-2,2-dimethyl-2H-chromen-6-yl)-1-phenylpropan-1-one	yes	up
pos_2430	metab_2410	C41H78NO8P	PC(15:0/18:2(9Z,12Z))	yes	up
pos_2452	metab_2432	C44H80NO7P	PC(P-16:0/20:4)	yes	up
pos_2741	metab_2721	C19H28O3S	S-Japonin	yes	up
pos_3065	metab_3041	C16H32O3	3-hydroxy-hexadecanoic acid	yes	up
pos_3090	metab_3066	C17H34O4	MG(14:0/0:0/0:0)	yes	up
pos_3469	metab_3442	C13H25NO4	(+/-)-Hexanoylcarnitine	yes	up
pos_3542	metab_3512	C4H9N3O2	Creatine	yes	up
pos_4131	metab_4063	C11H21NO5	(R)-3-hydroxybutyrylcarnitine	yes	up
pos_7287	metab_7124	C12H20O2	8-Dodecynoic acid	yes	up
pos_7691	metab_7525	C11H18O2	Methyl 4,8-decadienoate	yes	up
pos_7754	metab_7588	C12H18O3	Jasmonic acid	yes	up
pos_8214	metab_8046	C14H24O2	Alepric acid	yes	up
pos_8249	metab_8080	C10H18O	2-decenal	yes	up
pos_12338	metab_12083	C20H30O7	Cinncassiol A	yes	up
pos_12881	metab_12595	C27H44O3	23S,25-dihydroxyvitamin D3	yes	up
pos_13098	metab_12808	C14H22	3,5,7-Trimethyl-2E,4E,6E,8E-undecatetraene	yes	up
pos_13600	metab_13298	C12H20O	3,6,8-dodecatrien-1-ol	yes	up
pos_13753	metab_13449	C19H26O3	Acitretin(Ro 23-3571)	yes	up
pos_13827	metab_13522	C31H45NO5	Scyphostatin A	yes	up
pos_14037	metab_13730	C8H8O	Phenylacetaldehyde	yes	up
pos_14166	metab_13857	C11H18O2	Methyl geranate	yes	up

Table S1 Plasma Metabolomics (continued)

ID	Metab ID	Formula	Metabolite	Significant	Regulate
pos_14180	metab_13871	C22H28O4	Nitenin	yes	up
pos_14393	metab_14082	C13H14O	(E)-2-Tridecene-4,6,8-triyn-1-ol	yes	up
pos_14420	metab_14109	C18H26O4	Compactin diol lactone	yes	up
pos_14575	metab_14261	C17H33NO4	Decanoyl-L-carnitine	yes	up
pos_14771	metab_14455	C12H16O2	C12:4n-2,4,8,10	yes	up
pos_15520	metab_15200	C17H28O4	(1(10)E,4a,5E)-1(10),5-Germacradiene-12-acetoxy-4,11-diol	yes	up
pos_15795	metab_15459	C11H12O4	Dimethylcaffeic acid	yes	up
pos_16702	metab_16345	C15H24O4	Bisacurone epoxide	yes	up
pos_18520	metab_18142	C14H18N2O4	L-phenylalanyl-L-hydroxyproline	yes	up
pos_19521	metab_19109	C6H11NO4	Acetylhomoserine	yes	up
pos_19712	metab_19294	C4H6O2	Oxolan-3-one	yes	up
pos_19899	metab_19464	C9H17NO4	Acetylcarnitine	yes	up
pos_20160	metab_19698	C7H15NO3	L-Carnitine	yes	up
pos_809	metab_20185	C19H30O2	Epiandrosterone	yes	up
pos_607	metab_603	C46H84NO8P	PC(18:1(11Z)/20:3(5Z,8Z,11Z))	yes	down
pos_1129	metab_1118	C7H8N2O2	N-Methyl-4-pyridone-3-carboxamide	yes	down
pos_2429	metab_2409	C48H82NO8P	PC(20:3(5Z,8Z,11Z)/20:4(8Z,11Z,14Z,17Z))	yes	down
pos_2887	metab_2866	C28H52NO7P	PC(20:3/0:0)	yes	down
pos_3055	metab_3031	C14H22O3	(9R,13R)-1a,1b-dihomo-jasmonic acid	yes	down
pos_13673	metab_13371	C18H35NO2	Lepadin D	yes	down

Table S2 Liver Metabolomics

ID	Metab ID	Formula	Metabolite	Significant	Regulate
neg_18	metab_17855	C20H34O7	10,11-dihydro-20-trihydroxy-leukotriene B4	yes	up
neg_529	metab_18351	C21H36O9	Glucosyl (2E,6E,10x)-10,11-dihydroxy-2,6-farnesadienoate	yes	up
neg_1548	metab_19358	C4H9N3O2	3-Guanidinopropanoate	yes	up
neg_2440	metab_20195	C10H16O4	Alpha-Carboxy-delta-nonalactone	yes	up
neg_2515	metab_20264	C16H25NO9	Simmondsin	yes	up
neg_2825	metab_20571	C14H18N2O5	Tyrosyl-Hydroxyproline	yes	up
neg_2840	metab_20586	C11H20O6	Prenyl glucoside	yes	up
neg_3190	metab_20933	C9H12O2	2,6,6-Trimethyl-2-cyclohexene-1,4-dione	yes	up
neg_4246	metab_21976	C14H26O5	3-Hydroxytetradecanedioic acid	yes	up
neg_4867	metab_22587	C25H38O6	Erinacine C	yes	up
neg_5721	metab_23421	C25H42NO7P	PE(20:5/0:0)	yes	up
neg_7931	metab_25570	C21H44NO6P	PE(P-16:0e/0:0)	yes	up
neg_8088	metab_25712	C27H48NO7P	PE(22:4/0:0)	yes	up
neg_8231	metab_25842	C27H46NO7P	PE(22:5/0:0)	yes	up
neg_8448	metab_26046	C23H44NO7P	PE(18:2/0:0)	yes	up
neg_8800	metab_26383	C23H42NO7P	LysoPE(0:0/18:3(9Z,12Z,15Z))	yes	up
neg_9201	metab_26771	C25H36O6	Erinacine B	yes	up
neg_10841	metab_28379	C7H12O	Xi-3-Methyl-3-cyclohexen-1-ol	yes	up
neg_11179	metab_28716	C14H24O3	L-Menthyl acetoacetate	yes	up
neg_11264	metab_28801	C15H22O4	Arlatin	yes	up
neg_12588	metab_30114	C16H23N3O10	3'-Amino-3'-deoxythimidine glucuronide	yes	up
neg_12610	metab_30136	C21H22O5	3-[2-(hydroxymethyl)-5-methoxy-2-methyl-2H-chromen-6-yl]-1-(4-hydroxyphenyl)propan-1-one	yes	up
neg_76	metab_17911	C20H34O5	13,14-dihydro-15-keto-PGE1	yes	down
neg_139	metab_17974	C20H30O2	5,6-dehydro Arachidonic Acid	yes	down
neg_1270	metab_19083	C20H36O4	Prostaglandin D1 Alcohol	yes	down
neg_8334	metab_25939	C26H40N4O6	Neuromedin N (1-4)	yes	down
neg_8337	metab_25942	C21H32O4	3b,15b,17a-Trihydroxy-pregnenone	yes	down
neg_9081	metab_26657	C20H34O3	8(S)-HETrE	yes	down
neg_9140	metab_26713	C21H34O5	Cortolone	yes	down
neg_9592	metab_27148	C24H40O6	1b-Hydroxycholic acid	yes	down
neg_10008	metab_27556	C22H34O5	8-iso-16-cyclohexyl-tetranor Prostaglandin E2	yes	down
pos_104	metab_103	C12H20O2	3,7-Dimethyl-2E,6-octadienyl acetate	yes	up
pos_163	metab_162	C20H28O	9-cis-retinal	yes	up
pos_276	metab_274	C19H28O4	Oryzalide B	yes	up
pos_306	metab_304	C27H44NO7P	PE(22:6/0:0)	yes	up
pos_442	metab_438	C20H28O4	7'-Carboxy-gamma-tocotrienol	yes	up
pos_671	metab_665	C21H44NO6P	PE(P-16:0/0:0)	yes	up

Table S2 Liver Metabolomics (continued)

ID	Metab ID	Formula	Metabolite	Significant	Regulate
pos_1092	metab_1077	C21H30O4	21-Deoxycortisol	yes	up
pos_1104	metab_1089	C21H32O4	15(R)-15-methyl Prostaglandin A2	yes	up
pos_1718	metab_1690	C20H26O3	4-Oxo-13-cis-retinoate	yes	up
pos_2151	metab_2122	C41H76NO8P	GPEtn(18:1/18:2)	yes	up
pos_2189	metab_2160	C43H78NO7P	PE(P-18:0/20:4)	yes	up
pos_2388	metab_2358	C44H80NO7P	PC(P-16:0/20:4)	yes	up
pos_2861	metab_2826	C23H42NO7P	PE(18:3/0:0)	yes	up
pos_4896	metab_4794	C6H10O4S	3,3'-Thiobispropanoic acid	yes	up
pos_6730	metab_6621	C20H26O3	All-trans-4-oxoretinoic acid	yes	up
pos_8589	metab_8451	C45H76NO8P	GPEtn(18:1/22:6)	yes	up
pos_13153	metab_12910	C14H24O3	(1S,2S)-3-oxo-2-pentyl-cyclopentanebutanoic acid	yes	up
pos_13222	metab_12979	C20H28O4	5,6-epoxy,18R-HEPE	yes	up
pos_8014	metab_17836	C20H30O	Retinol	yes	up
pos_19	metab_18	C19H36O4	MG(16:1(9Z)/0:0/0:0)	yes	down
pos_46	metab_45	C18H36O4	(+)-15,16-Dihydroxyoctadecanoic acid	yes	down
pos_134	metab_133	C37H66O5	DG(16:1(9Z)/18:2(9Z,12Z)/0:0)	yes	down
pos_136	metab_135	C37H68O5	DG(18:2(9Z,12Z)/16:0/0:0)	yes	down
pos_165	metab_164	C22H32O3	(+/-)13-HDoHE	yes	down
pos_166	metab_165	C18H34O3	Ricinoleic acid	yes	down
pos_172	metab_171	C20H30O2	Eicosapentaenoic Acid	yes	down
pos_177	metab_176	C29H49O12P	PI(20:4(5Z,8Z,11Z,14Z)/0:0)	yes	down
pos_182	metab_181	C16H26O2	SCLAREOLIDE	yes	down
pos_336	metab_334	C15H26O3	8-Hydroxy-4(6)-lactarene-5,14-diol	yes	down
pos_548	metab_542	C35H64O5	DG(14:1(9Z)/18:1(11Z)/0:0)	yes	down
pos_1598	metab_1574	C8H15NO6	N-Acetylmannosamine	yes	down
pos_2179	metab_2150	C35H66O5	DG(16:0/16:1(9Z)/0:0)	yes	down
pos_2188	metab_2159	C46H86NO8P	PC(18:0/20:3(5Z,8Z,11Z))	yes	down
pos_2432	metab_2400	C50H82NO8P	PC(20:3(5Z,8Z,11Z)/22:6(4Z,7Z,10Z,13Z,16Z,19Z))	yes	down
pos_6451	metab_6344	C15H26N2O2	Aphyllic acid	yes	down
pos_6538	metab_6430	C21H24N2O4	Horhammericine	yes	down
pos_7587	metab_7473	C19H32O2	Methyl linolenate	yes	down
pos_9239	metab_9090	C18H34O2	Vaccenic acid	yes	down
pos_9964	metab_9800	C39H66O5	DG(18:2(9Z,12Z)/18:3(9Z,12Z,15Z)/0:0)	yes	down
pos_11192	metab_10981	C21H24O4	5-Deoxymyricanone	yes	down
pos_11943	metab_11706	C22H36O3	Carbocyclic Thromboxane A2	yes	down
pos_11972	metab_11735	C20H34O3	15-OxoEDE	yes	down
pos_12032	metab_11794	C22H32O3	1alpha-hydroxy-22-oxo-23,24,25,26,27-pentanorvitamin D3	yes	down
pos_1429	metab_17831	C12H22O11	Inulobiose	yes	down

Table S3 RNA-seq

Gene id	Gene name	Gene description	T_Ctrl_ vs_T_GHB
306			
ENSMUSG00000053219	Raet1e	retinoic acid early transcript 1E	Down
ENSMUSG00000009633	G0s2	G0/G1 switch gene 2	Down
ENSMUSG00000042195	Slc35f2	solute carrier family 35, member F2	Down
ENSMUSG00000073835	Mup-ps12	major urinary protein, pseudogene 12	Down
ENSMUSG00000050860	Phospho1	phosphatase, orphan 1	Down
ENSMUSG00000089929	Bcl2a1b	B cell leukemia/lymphoma 2 related protein A1b	Down
ENSMUSG00000049685	Cyp2g1	cytochrome P450, family 2, subfamily g, polypeptide 1	Down
ENSMUSG00000079242	C730034F03Rik	RIKEN cDNA C730034F03 gene	Down
ENSMUSG00000000440	Pparg	peroxisome proliferator activated receptor gamma	Down
ENSMUSG00000109141	Gm30692	predicted gene, 30692	Down
ENSMUSG00000030364	Clec2h	C-type lectin domain family 2, member h	Down
ENSMUSG00000030762	Aqp8	aquaporin 8	Down
ENSMUSG00000081094	Rpl19-ps11	ribosomal protein L19, pseudogene 11	Down
ENSMUSG00000092323	BB365896	expressed sequence BB365896	Down
ENSMUSG00000110597	Gm8798	predicted gene 8798	Down
ENSMUSG00000087404	Gm11752	predicted gene 11752	Down
ENSMUSG00000092517	Art2a	ADP-ribosyltransferase 2a	Down
ENSMUSG00000019214	Chtf18	CTF18, chromosome transmission fidelity factor 18	Down
ENSMUSG00000030468	Siglecg	sialic acid binding Ig-like lectin G	Down
ENSMUSG00000083171	Gm12321	predicted gene 12321	Down
ENSMUSG00000078735	Il11ra2	interleukin 11 receptor, alpha chain 2	Down
ENSMUSG00000090622	A930033H14Rik	RIKEN cDNA A930033H14 gene	Down
ENSMUSG00000029822	Osbpl3	oxysterol binding protein-like 3	Down
ENSMUSG00000106224	Gm43823	predicted gene 43823	Down
ENSMUSG00000094437	Gm9830	predicted gene 9830	Down
ENSMUSG00000032643	Fhl3	four and a half LIM domains 3	Down
ENSMUSG00000112384	Gm34921	predicted gene, 34921	Down
ENSMUSG00000035186	Ubd	ubiquitin D	Down
ENSMUSG00000029254	Stap1	signal transducing adaptor family member 1	Down
ENSMUSG00000097352	C920009B18Rik	RIKEN cDNA C920009B18 gene	Down
ENSMUSG00000004654	Ghrhr	growth hormone releasing hormone receptor	Down
ENSMUSG00000050578	Mmp13	matrix metallopeptidase 13	Down
ENSMUSG00000068220	Lgals1	lectin, galactose binding, soluble 1	Down
ENSMUSG00000041653	Pnpla3	patatin-like phospholipase domain containing 3	Down
ENSMUSG00000096458	Moap1	modulator of apoptosis 1	Down

Table S3 RNA-seq (continued)

Gene id	Gene name	Gene description	T_Ctrl_ vs_T_GHB
ENSMUSG00000046415	B430212C06Rik	RIKEN cDNA B430212C06 gene	Down
ENSMUSG00000118011	Gm50266	predicted gene, 50266	Down
ENSMUSG00000031636	Pdlim3	PDZ and LIM domain 3	Down
ENSMUSG00000044017	Adgrd1	adhesion G protein-coupled receptor D1	Down
ENSMUSG00000093930	Hmgcs1	3-hydroxy-3-methylglutaryl-Coenzyme A synthase 1	Down
ENSMUSG00000068601	Gm10244	predicted gene 10244	Down
ENSMUSG00000061086	Myl4	myosin, light polypeptide 4	Down
ENSMUSG00000100157	2310034O05Rik	RIKEN cDNA 2310034O05 gene	Down
ENSMUSG00000100254	Trpc2	transient receptor potential cation channel, subfamily C, member 2	Down
ENSMUSG00000099889	Mrgprb11-ps	MAS-related GPR, member B11, pseudogene	Down
ENSMUSG00000040592	Cd79b	CD79B antigen	Down
ENSMUSG00000028773	Fabp3	fatty acid binding protein 3	Down
ENSMUSG00000070713	Gm10282	predicted pseudogene 10282	Down
ENSMUSG00000049723	Mmp12	matrix metallopeptidase 12	Down
ENSMUSG00000028871	Rspo1	R-spondin 1	Down
ENSMUSG00000055809	Dnaaf3	dynein, axonemal assembly factor 3	Down
ENSMUSG00000041538	H2-Ob	histocompatibility 2, O region beta locus	Down
ENSMUSG00000001739	Cldn15	claudin 15	Down
ENSMUSG00000069170	Adgrv1	adhesion G protein-coupled receptor V1	Down
ENSMUSG00000102615	Gm37844	predicted gene, 37844	Down
ENSMUSG00000062170	Fmr1nb	Fmr1 neighbor	Down
ENSMUSG00000110838	Gm47789	predicted gene, 47789	Down
ENSMUSG00000107198	Gm19619	predicted gene, 19619	Down
ENSMUSG00000091462	Gm17084	predicted gene 17084	Down
ENSMUSG00000028671	Gale	galactose-4-epimerase, UDP	Down
ENSMUSG00000114247	Gm32063	predicted gene, 32063	Down
ENSMUSG00000030724	Cd19	CD19 antigen	Down
ENSMUSG00000063011	Msln	mesothelin	Down
ENSMUSG00000001131	Timp1	tissue inhibitor of metalloproteinase 1	Down
ENSMUSG00000116656	Gm49708	predicted gene, 49708	Down
ENSMUSG00000022696	Sidt1	SID1 transmembrane family, member 1	Down
ENSMUSG00000027574	Nkain4	Na+/K+ transporting ATPase interacting 4	Down
ENSMUSG00000027577	Chrna4	cholinergic receptor, nicotinic, alpha polypeptide 4	Down
ENSMUSG00000040985	Sun3	Sad1 and UNC84 domain containing 3	Down
ENSMUSG00000110774	Gm39318	predicted gene, 39318	Down

Table S3 RNA-seq (continued)

Gene id	Gene name	Gene description	T_Ctrl_ vs_T_GHB
ENSMUSG00000112110	Gm15608	predicted gene 15608	Down
ENSMUSG00000001349	Cnn1	calponin 1	Down
ENSMUSG00000086015	4833417C18Rik	RIKEN cDNA 4833417C18 gene	Down
ENSMUSG00000038508	Gdf15	growth differentiation factor 15	Down
ENSMUSG00000061780	Cfd	complement factor D (adipsin)	Down
ENSMUSG00000026650	Meig1	meiosis expressed gene 1	Down
ENSMUSG00000113811	Gm47882	predicted gene, 47882	Down
ENSMUSG00000004341	Gpx6	glutathione peroxidase 6	Down
ENSMUSG00000073460	Pnldc1	poly(A)-specific ribonuclease (PARN)-like domain containing 1	Down
ENSMUSG00000097253	Gm26770	predicted gene, 26770	Down
ENSMUSG00000028664	Ephb2	Eph receptor B2	Down
ENSMUSG00000057969	Sema3b	sema domain, immunoglobulin domain (Ig), short basic domain, secreted, (semaphorin) 3B	Down
ENSMUSG00000002944	Cd36	CD36 molecule	Down
ENSMUSG00000114469	C730002L08Rik	RIKEN cDNA C730002L08 gene	Down
ENSMUSG00000025726	Slc28a1	solute carrier family 28 (sodium-coupled nucleoside transporter), member 1	Down
ENSMUSG00000090002	Gm16006	predicted gene 16006	Down
ENSMUSG00000021950	Anxa8	annexin A8	Down
ENSMUSG00000032254	Kif23	kinesin family member 23	Down
ENSMUSG00000006398	Cdc20	cell division cycle 20	Down
ENSMUSG00000110755	BC049987	cDNA sequence BC049987	Down
ENSMUSG00000114664	Gm48639	predicted gene, 48639	Down
ENSMUSG00000115509	Gm49012	predicted gene, 49012	Down
ENSMUSG00000058794	Nfe2	nuclear factor, erythroid derived 2	Down
ENSMUSG00000030278	Cidec	cell death-inducing DFFA-like effector c	Down
ENSMUSG00000006517	Mvd	mevalonate (diphospho) decarboxylase	Down
ENSMUSG00000103144	Pcdhga1	protocadherin gamma subfamily A, 1	Down
ENSMUSG00000032080	Apoa4	apolipoprotein A-IV	Down
ENSMUSG00000012187	Mogat1	monoacylglycerol O-acyltransferase 1	Down
ENSMUSG00000034634	Ly6d	lymphocyte antigen 6 complex, locus D	Down
ENSMUSG00000044854	1700056E22Rik	RIKEN cDNA 1700056E22 gene	Down
ENSMUSG00000048489	Depp1	DEPP1 autophagy regulator	Down
ENSMUSG00000011008	Mcoln2	mucolipin 2	Down
ENSMUSG00000018868	Pnpla5	patatin-like phospholipase domain containing 5	Down
ENSMUSG00000038768	9130409I23Rik	RIKEN cDNA 9130409I23 gene	Down
ENSMUSG00000112762	4930459C07Rik	RIKEN cDNA 4930459C07 gene	Down

Table S3 RNA-seq (continued)

Gene id	Gene name	Gene description	T_Ctrl_ vs_T_GHB
ENSMUSG00000005883	Spo11	SPO11 initiator of meiotic double stranded breaks	Down
ENSMUSG00000030789	Itgax	integrin alpha X	Down
ENSMUSG00000058672	Tubb2a	tubulin, beta 2A class IIA	Down
ENSMUSG00000005540	Fcer2a	Fc receptor, IgE, low affinity II, alpha polypeptide	Down
ENSMUSG00000044678	Ly6k	lymphocyte antigen 6 complex, locus K	Down
ENSMUSG00000091867	Cyp2a22	cytochrome P450, family 2, subfamily a, polypeptide 22	Down
ENSMUSG00000083812	Gm5054	predicted gene 5054	Down
ENSMUSG00000021872	Rnase10	ribonuclease, RNase A family, 10 (non-active)	Down
ENSMUSG00000110611	Gm20163	predicted gene, 20163	Down
ENSMUSG00000107019	Gm43682	predicted gene 43682 [Source:MGI Symbol	Down
ENSMUSG00000021974	Fgf9	fibroblast growth factor 9	Down
ENSMUSG00000111282	Gm47528	predicted gene, 47528	Down
ENSMUSG00000001403	Ube2c	ubiquitin-conjugating enzyme E2C	Down
ENSMUSG00000038352	Arl5c	ADP-ribosylation factor-like 5C	Down
ENSMUSG00000108472	Gm45212	predicted gene 45212	Down
ENSMUSG00000055745	Rtl6	retrotransposon Gag like 6	Down
ENSMUSG00000089665	Fcor	Foxo1 corepressor	Down
ENSMUSG00000087669	Gm11724	predicted gene 11724	Down
ENSMUSG00000038540	Tmc3	transmembrane channel-like gene family 3	Down
ENSMUSG00000020419	Hormad2	HORMA domain containing 2	Down
ENSMUSG00000020651	Slc26a4	solute carrier family 26, member 4	Down
ENSMUSG00000097533	Gm26590	predicted gene, 26590	Down
ENSMUSG00000075025	Gm10804	predicted gene 10804	Down
ENSMUSG00000022033	Pbk	PDZ binding kinase	Down
ENSMUSG00000049109	Themis	thymocyte selection associated	Down
ENSMUSG00000008153	Clstn3	calsyntenin 3	Down
ENSMUSG00000087611	4930458D05Rik	RIKEN cDNA 4930458D05 gene	Down
ENSMUSG00000098140	Gm26938	predicted gene, 26938	Down
ENSMUSG00000043259	Fam13c	family with sequence similarity 13, member C	Down
ENSMUSG00000024526	Cidea	cell death-inducing DNA fragmentation factor, alpha subunit-like effector A	Down
ENSMUSG00000104213	Ighd	immunoglobulin heavy constant delta	Down
ENSMUSG00000078452	Raet1d	retinoic acid early transcript delta	Down
ENSMUSG00000021200	Asb2	ankyrin repeat and SOCS box-containing 2	Down
ENSMUSG00000075044	Slc22a29	solute carrier family 22. member 29	Down
ENSMUSG00000111013	Gm32468	predicted gene, 32468	Down

Table S3 RNA-seq (continued)

Gene id	Gene name	Gene description	T_Ctrl_ vs_T_GHB
ENSMUSG00000038725	Pkhd1l1	polycystic kidney and hepatic disease 1-like 1	Down
ENSMUSG00000086136	Gm12718	predicted gene 12718	Down
ENSMUSG00000042985	Upk3b	uroplakin 3B	Down
ENSMUSG00000097762	4732463B04Rik	RIKEN cDNA 4732463B04 gene	Down
ENSMUSG00000099570	Gm29000	predicted gene 29000	Down
ENSMUSG00000118383	Gm50321	predicted gene, 50321	Down
ENSMUSG00000097482	Gm17634	predicted gene, 17634	Down
ENSMUSG00000116295	Gm32885	predicted gene, 32885	Down
ENSMUSG00000082920	Gm13864	predicted gene 13864	Down
ENSMUSG00000062309	Rpp25	ribonuclease P/MRP 25 subunit	Down
ENSMUSG00000107252	Gm5767	predicted gene 5767	Down
ENSMUSG00000052485	Tmem171	transmembrane protein 171	Down
ENSMUSG00000037953	A4gnt	alpha-1,4-N-acetylglucosaminyltransferase	Down
ENSMUSG00000033450	Tagap	T cell activation Rho GTPase activating protein	Down
ENSMUSG00000074570	Cass4	Cas scaffolding protein family member 4	Down
ENSMUSG00000116478	Gm18890	predicted gene, 18890	Down
ENSMUSG00000035385	Ccl2	chemokine (C-C motif) ligand 2	Down
ENSMUSG00000067818	Myl9	myosin, light polypeptide 9, regulatory	Down
ENSMUSG00000074183	Gsta1	glutathione S-transferase, alpha 1 (Ya)	Down
ENSMUSG00000070425	Xntrpc	Xndc1-transient receptor potential cation channel, subfamily C, member 2 readthrough	Up
ENSMUSG00000097140	Gm26779	predicted gene, 26779	Up
ENSMUSG00000049892	Rasd1	RAS, dexamethasone-induced 1	Up
ENSMUSG00000083012	Fam220a	family with sequence similarity 220, member A	Up
ENSMUSG00000101596	Gm28182	predicted gene 28182	Up
ENSMUSG00000110440	Gm45894	predicted gene 45894	Up
ENSMUSG00000064357	mt-Atp6	mitochondrially encoded ATP synthase 6	Up
ENSMUSG00000104159	Gm38099	predicted gene, 38099	Up
ENSMUSG00000047511	Olfr1396	olfactory receptor 1396	Up
ENSMUSG00000017146	Brca1	breast cancer 1, early onset	Up
ENSMUSG00000113898	Gm19144	predicted gene, 19144	Up
ENSMUSG00000115272	Gm49965	predicted gene, 49965	Up
ENSMUSG00000074115	Saa1	serum amyloid A 1	Up
ENSMUSG00000029683	Lmod2	leiomodin 2 (cardiac)	Up
ENSMUSG00000105891	A230001M10Rik	RIKEN cDNA A230001M10 gene	Up
ENSMUSG00000001672	Marveld3	MARVEL (membrane-associating) domain containing 3	Up

Table S3 RNA-seq (continued)

Gene id	Gene name	Gene description	T_Ctrl_ vs_T_GHB
ENSMUSG00000040017	Saa4	serum amyloid A 4	Up
ENSMUSG00000061322	Dnai1	dynein axonemal intermediate chain 1	Up
ENSMUSG00000044927	H1f10	H1.10 linker histone	Up
ENSMUSG00000110384	Gm45301	predicted gene 45301	Up
ENSMUSG00000092009	Myh15	myosin, heavy chain 15	Up
ENSMUSG00000085615	A330035P11Rik	RIKEN cDNA A330035P11 gene	Up
ENSMUSG00000032482	Cspg5	chondroitin sulfate proteoglycan 5	Up
ENSMUSG00000108884	Gm45792	predicted gene 45792	Up
ENSMUSG00000083170	Gm14405	predicted gene 14405	Up
ENSMUSG00000021466	Ptch1	patched 1	Up
ENSMUSG00000074269	Rec114	REC114 meiotic recombination protein	Up
ENSMUSG00000091971	Hspa1a	heat shock protein 1A	Up
ENSMUSG00000117001	Gm49858	predicted gene, 49858	Up
ENSMUSG00000048794	Cfap100	cilia and flagella associated protein 100	Up
ENSMUSG00000029380	Cxcl1	chemokine (C-X-C motif) ligand 1	Up
ENSMUSG00000024222	Fkbp5	FK506 binding protein 5	Up
ENSMUSG00000092470	Gm20518	predicted gene 20518	Up
ENSMUSG00000117250	Gm49871	predicted gene, 49871	Up
ENSMUSG00000113399	Gm48199	predicted gene, 48199	Up
ENSMUSG00000001095	Slc13a2	solute carrier family 13 (sodium-dependent dicarboxylate transporter), member 2	Up
ENSMUSG00000104113	Gm37292	predicted gene, 37292	Up
ENSMUSG00000094098	Vmn2r44	vomeronasal 2, receptor 44	Up
ENSMUSG00000084917	Gm17477	predicted gene, 17477	Up
ENSMUSG00000104918	Gm42944	predicted gene 42944	Up
ENSMUSG00000039903	Eva1c	eva-1 homolog C (C. elegans)	Up
ENSMUSG00000037443	Cep85	centrosomal protein 85	Up
ENSMUSG00000037447	Arid5a	AT rich interactive domain 5A (MRF1-like)	Up
ENSMUSG00000107877	Gm43951	predicted gene, 43951	Up
ENSMUSG00000100150	Gm19585	predicted gene, 19585	Up
ENSMUSG00000084383	Gm13370	predicted gene 13370	Up
ENSMUSG00000038415	Foxq1	forkhead box Q1	Up
ENSMUSG00000099556	Gm28857	predicted gene 28857	Up
ENSMUSG00000113261	Gm47404	predicted gene, 47404	Up
ENSMUSG00000097443	Gm17529	predicted gene, 17529	Up
ENSMUSG00000115220	Gm49768	predicted gene, 49768	Up

Table S3 RNA-seq (continued)

Gene id	Gene name	Gene description	T_Ctrl_ vs_T_GHB
ENSMUSG00000066361	Serpina3c	serine (or cysteine) peptidase inhibitor, clade A, member 3C	Up
ENSMUSG00000020000	Moxd1	monooxygenase, DBH-like 1	Up
ENSMUSG00000057465	Saa2	serum amyloid A 2	Up
ENSMUSG00000104222	Gm7292	predicted gene 7292	Up
ENSMUSG00000020218	Wif1	Wnt inhibitory factor 1	Up
ENSMUSG00000051639	Fbl-ps2	fibrillarin, pseudogene 2	Up
ENSMUSG00000060716	Plekhh1	pleckstrin homology domain containing, family H (with MyTH4 domain) member 1	Up
ENSMUSG00000109863	Gm45643	predicted gene 45643	Up
ENSMUSG00000028354	Fmn2	formin 2	Up
ENSMUSG00000109807	Gm45244	predicted gene 45244	Up
ENSMUSG00000025582	Nptx1	neuronal pentraxin 1	Up
ENSMUSG00000047462	Gpr141b	G protein-coupled receptor 141B	Up
ENSMUSG00000020805	Slc13a5	solute carrier family 13 (sodium-dependent citrate transporter), member 5	Up
ENSMUSG00000037341	Slc9a7	solute carrier family 9 (sodium/hydrogen exchanger), member 7	Up
ENSMUSG00000050440	Hamp	hepcidin antimicrobial peptide	Up
ENSMUSG00000056966	Gjc3	gap junction protein, gamma 3	Up
ENSMUSG00000027070	Lrp2	low density lipoprotein receptor-related protein 2	Up
ENSMUSG00000042846	Lrrtm3	leucine rich repeat transmembrane neuronal 3	Up
ENSMUSG00000026072	Il1r1	interleukin 1 receptor, type I	Up
ENSMUSG00000116765	Gm49762	predicted gene, 49762	Up
ENSMUSG00000029752	Asns	asparagine synthetase	Up
ENSMUSG00000072849	Serpina1e	serine (or cysteine) peptidase inhibitor, clade A, member 1E	Up
ENSMUSG00000030219	Erp27	endoplasmic reticulum protein 27	Up
ENSMUSG00000103560	Gm38070	predicted gene, 38070	Up
ENSMUSG00000024873	Cnih2	cornichon family AMPA receptor auxiliary protein 2	Up
ENSMUSG00000105703	Gm43305	predicted gene 43305	Up
ENSMUSG00000026415	Fcamr	Fc receptor, IgA, IgM, high affinity	Up
ENSMUSG00000105708	Gm36070	predicted gene, 36070	Up
ENSMUSG00000024274	Zscan30	zinc finger and SCAN domain containing 30	Up
ENSMUSG00000108878	Gm49493	predicted gene, 49493	Up
ENSMUSG00000070501	Ifi214	interferon activated gene 214	Up
ENSMUSG00000053113	Socs3	suppressor of cytokine signaling 3	Up
ENSMUSG00000091680	Klhdc7b	kelch domain containing 7B	Up
ENSMUSG00000105338	Gm43802	predicted gene 43802	Up
ENSMUSG00000076576	Igkv6-32	immunoglobulin kappa variable 6-32	Up

Table S3 RNA-seq (continued)

Gene id	Gene name	Gene description	T_Ctrl_ vs_T_GHB
ENSMUSG00000087367	Gm15491	predicted gene 15491	Up
ENSMUSG00000020185	E2f7	E2F transcription factor 7	Up
ENSMUSG00000101106	Gm28819	predicted gene 28819	Up
ENSMUSG00000001103	Sebox	SEBOX homeobox	Up
ENSMUSG00000005952	Trpv1	transient receptor potential cation channel, subfamily V, member 1	Up
ENSMUSG00000038599	Capn8	calpain 8	Up
ENSMUSG00000049281	Scn3b	sodium channel, voltage-gated, type III, beta	Up
ENSMUSG00000100162	Gm20687	predicted gene 20687	Up
ENSMUSG00000058579	Cela2a	chymotrypsin-like elastase family, member 2A	Up
ENSMUSG00000085445	Gm16348	predicted gene 16348	Up
ENSMUSG00000022388	Ttll8	tubulin tyrosine ligase-like family, member 8	Up
ENSMUSG00000096883	Shisa8	shisa family member 8	Up
ENSMUSG00000021209	Ppp4r4	protein phosphatase 4, regulatory subunit 4	Up
ENSMUSG00000113663	Gm48504	predicted gene, 48504	Up
ENSMUSG00000100968	Gm2098	predicted gene 2098	Up
ENSMUSG00000020205	Phlda1	pleckstrin homology like domain, family A, member 1	Up
ENSMUSG00000086765	Gm11827	predicted gene 11827	Up
ENSMUSG00000116946	Gm41442	predicted gene, 41442	Up
ENSMUSG00000026442	Nfasc	neurofascin	Up
ENSMUSG00000057425	Ugt2b37	UDP glucuronosyltransferase 2 family, polypeptide B37	Up
ENSMUSG00000028862	Map3k6	mitogen-activated protein kinase kinase kinase 6	Up
ENSMUSG00000024029	Tff3	trefoil factor 3, intestinal	Up
ENSMUSG00000037386	Rims2	regulating synaptic membrane exocytosis 2	Up
ENSMUSG00000116145	5730521K06Rik	RIKEN cDNA 5730521K06 gene	Up
ENSMUSG00000021750	Fam107a	family with sequence similarity 107, member A	Up
ENSMUSG00000021453	Gadd45g	growth arrest and DNA-damage-inducible 45 gamma	Up
ENSMUSG00000066687	Zbtb16	zinc finger and BTB domain containing 16	Up
ENSMUSG00000041930	Fam222a	family with sequence similarity 222, member A	Up
ENSMUSG00000030650	Tmc5	transmembrane channel-like gene family 5	Up
ENSMUSG00000083287	Idi1-ps1	isopentenyl-diphosphate delta isomerase, pseudogene 1	Up
ENSMUSG00000040125	Gpr26	G protein-coupled receptor 26	Up
ENSMUSG00000098678	Mroh6	maestro heat-like repeat family member 6	Up
ENSMUSG00000109198	D7Bwg0826e	DNA segment, Chr 7, Brigham & Women's Genetics 0826 expressed	Up
ENSMUSG00000090021	Gm6493	predicted gene 6493	Up
ENSMUSG00000095061	E030018B13Rik	RIKEN cDNA E030018B13 gene	Up

Table S3 RNA-seq (continued)

Gene id	Gene name	Gene description	T_Ctrl_ vs_T_GHB
ENSMUSG00000049414	Gm5417	predicted gene 5417	Up
ENSMUSG00000090264	Eif4ebp3	eukaryotic translation initiation factor 4E binding protein 3	Up
ENSMUSG00000048534	Jaml	junction adhesion molecule like	Up
ENSMUSG00000052415	Tchh	trichohyalin	Up
ENSMUSG00000022032	Scara5	scavenger receptor class A, member 5	Up
ENSMUSG00000091393	5330438I03Rik	RIKEN cDNA 5330438I03 gene	Up
ENSMUSG00000030483	Cyp2b10	cytochrome P450, family 2, subfamily b, polypeptide 10	Up
ENSMUSG00000042918	Mamstr	MEF2 activating motif and SAP domain containing transcriptional regulator	Up
ENSMUSG00000071036	Gm10309	predicted gene 10309	Up
ENSMUSG00000117901		novel transcript, antisense to Macrod1	Up
ENSMUSG00000090069	E430024P14Rik	RIKEN cDNA E430024P14 gene	Up
ENSMUSG00000058921	Slc10a5	solute carrier family 10 (sodium/bile acid cotransporter family), member 5	Up
ENSMUSG00000028445	Enho	energy homeostasis associated	Up
ENSMUSG00000022346	Myc	myelocytomatosis oncogene	Up
ENSMUSG00000038037	Socs1	suppressor of cytokine signaling 1	Up
ENSMUSG00000087684	1200007C13Rik	RIKEN cDNA 1200007C13 gene	Up
ENSMUSG00000072919	Noxred1	NADP+ dependent oxidoreductase domain containing 1	Up
ENSMUSG00000015533	Itga2	integrin alpha 2	Up
ENSMUSG00000066170	E230001N04Rik	RIKEN cDNA E230001N04 gene	Up
ENSMUSG00000057182	Scn3a	sodium channel, voltage-gated, type III, alpha	Up
ENSMUSG00000118670		mucin 19	Up
ENSMUSG00000056870	Gulp1	GULP, engulfment adaptor PTB domain containing 1	Up
ENSMUSG00000096221	1500002C15Rik	RIKEN cDNA 1500002C15 gene	Up
ENSMUSG00000092534	Pagr1b	PAXIP1 associated glutamate rich protein 1B	Up
ENSMUSG00000099389	Gm29603	predicted gene 29603	Up
ENSMUSG00000083992	Gm11478	predicted gene 11478	Up

Table S4 Plasma Metabolomics

Metabolites ID	Metabolite	Formula	Metab ID	Regulate
neg_1590	Erythronic acid	C4H8O5	metab_21744	down
neg_8994	Annoglabasin E	C20H32O3	metab_28653	down
neg_12734	9-Oxo-nonanoic acid	C9H16O3	metab_32064	down
neg_14055	2-O-(6-Phospho-alpha-mannosyl)-D-glycerate	C9H17O12P	metab_33271	down
pos_41	Linoleamide	C18H33NO	metab_40	down
pos_44	17,18-DiHETE	C20H32O4	metab_43	down
pos_59	(R)-(+)-2-Pyrrolidone-5-carboxylic acid	C5H7NO3	metab_58	down
pos_516	2,6-nonadienoic acid	C9H14O2	metab_512	down
pos_814	8-Hydroxy-4(6)-lactarene-5,14-diol	C15H26O3	metab_807	down
pos_830	(1S,2S)-3-oxo-2-pentyl-cyclopentanebutanoic acid	C14H24O3	metab_823	down
pos_839	7-oxo-11E,13-Tetradecadienoic acid	C14H22O3	metab_832	down
pos_840	3-Hydroxy-beta-ionone	C13H20O2	metab_833	down
pos_844	4,5-Dihydrovomifoliol	C13H22O3	metab_837	down
pos_852	7(14)-Bisabolene-2,3,10,11-tetrol	C15H28O4	metab_845	down
pos_2066	Zedoarondiol	C15H24O3	metab_2048	down
pos_2090	Prostaglandin-c2	C20H30O4	metab_2072	down
pos_2283	Farnesyl acetone	C18H30O	metab_2263	down
pos_3169	4-Hydroxyvalsartan	C24H29N5O4	metab_3143	down
pos_3641	Uric acid	C5H4N4O3	metab_3608	down
pos_5696	3-hydroxyhexanoyl carnitine	C14H27NO5	metab_5572	down
pos_5761	DL-2-Aminooctanoic acid	C8H17NO2	metab_5633	down
pos_8085	C16 Sphinganine	C16H35NO2	metab_7917	down
pos_13753	Acitretin(Ro 23-3571)	C19H26O3	metab_13449	down
pos_13971	Bremazocine	C20H29NO2	metab_13664	down
pos_14016	Vulgarone A	C15H22O	metab_13709	down
pos_14166	Methyl geranate	C11H18O2	metab_13857	down
pos_14180	Nitenin	C22H28O4	metab_13871	down
pos_14420	Compactin diol lactone	C18H26O4	metab_14109	down
pos_15116	8-Hydroxycarvotanacetone	C10H16O2	metab_14798	down
pos_16824	Dihydronepetalactone	C10H16O2	metab_16467	down
pos_16963	10-oxo-5,8-decadienoic acid	C10H14O3	metab_16606	down
pos_20073	L-Glutamine	C5H10N2O3	metab_19621	down
neg_1620	Butyl (S)-3-hydroxybutyrate [arabinosyl-(1->6)-glucoside]	C19H34O12	metab_21774	up
neg_2506	4-Nitrophenyl sulfate	C6H5NO6S	metab_22576	up
neg_4001	Goshonoside F4	C32H54O12	metab_23938	up
neg_5353	Saponin D	C48H78O17	metab_25160	up
neg_8621	Polyoxyethylene (600) monoricinoleate	C21H40O3	metab_28293	up
neg_11409	{[3-(2-hydroxy-4-methoxyphenyl)prop-2-en-1-yl]oxy} sulfonic acid	C10H12O6S	metab_30858	up

Table S5 Liver Metabolomics

ID	Metabolite	Metab ID	Formula	Regulate
neg_5987	9'-Carboxy-gamma-chromanol	metab_23678	C23H36O4	down
neg_6377	LysoPC(P-18:0)	metab_24041	C26H54NO6P	down
neg_9545	3'-Hydroxy-T2 Toxin	metab_27101	C24H34O10	down
neg_11996	5-[3-methoxy-4-(sulfooxy)phenyl]pentanoic acid	metab_29526	C12H16O7S	down
pos_126	Oleic Acid ethyl ester	metab_125	C20H38O2	down
pos_132	Arachidonic acid ethyl ester	metab_131	C22H36O2	down
pos_145	Arachidonic Acid methyl ester	metab_144	C21H34O2	down
pos_522	GPCho(20:4/22:6)	metab_516	C50H80NO8P	down
pos_529	GPCho(22:6/22:6)	metab_523	C52H80NO8P	down
pos_595	Cis-12-Octadecenoic Acid methyl ester	metab_589	C19H36O2	down
pos_1772	Sphinganine	metab_1744	C18H39NO2	down
pos_1810	N,N-dimethyl-Safingol	metab_1782	C20H43NO2	down
pos_2047	PC(20:0/0:0)	metab_2019	C28H58NO7P	down
pos_2089	PC(18:3(6Z,9Z,12Z)/22:6(4Z,7Z,10Z,13Z,16Z,19Z))	metab_2061	C48H78NO8P	down
pos_2097	GPEtn(20:4/22:6)	metab_2069	C47H74NO8P	down
pos_2102	PS(18:0/22:6(4Z,7Z,10Z,13Z,16Z,19Z))	metab_2074	C46H78NO10P	down
pos_2115	1alpha-hydroxy-25,26,27-trinorvitamin D3 24-carboxylic acid	metab_2087	C24H36O4	down
pos_2158	PC(P-18:0/18:3)	metab_2129	C44H82NO7P	down
pos_2429	PC(18:1(11Z)/18:3(9Z,12Z,15Z))	metab_2397	C44H80NO8P	down
pos_2432	PC(20:3(5Z,8Z,11Z)/22:6(4Z,7Z,10Z,13Z,16Z,19Z))	metab_2400	C50H82NO8P	down
pos_2437	GPEtn(18:2/22:6)	metab_2405	C45H74NO8P	down
pos_2438	PC(18:2(9Z,12Z)/22:6(4Z,7Z,10Z,13Z,16Z,19Z))	metab_2406	C48H80NO8P	down
pos_2611	PC(P-18:0/0:0)	metab_2579	C26H54NO6P	down
pos_3006	Sphingosine	metab_2969	C18H37NO2	down
pos_8789	PC(16:0/P-18:0)	metab_8643	C42H84NO7P	down
pos_10025	Lathosterol	metab_9856	C27H46O	down
pos_12379	Cerebronic acid	metab_12140	C24H48O3	down
pos_12591	MG(a-21:0/0:0/0:0)[rac]	metab_12352	C24H48O4	down
pos_15173	DL-2-Aminooctanoic acid	metab_14921	C8H17NO2	down
neg_55	Leucyl-phenylalanine	metab_17890	C15H22N2O3	up
neg_147	(+/-)4-HDoHE	metab_17982	C22H32O3	up
neg_194	N-Acetyl-D-phenylalanine	metab_18029	C11H13NO3	up
neg_642	(+/-)9-HpODE	metab_18463	C18H32O4	up
neg_2191	ALANYL-dl-LEUCINE	metab_19957	C9H18N2O3	up
neg_2292	8-(2-hydroxypropan-2-yl)-2-oxo-2H,8H,9H-furo[2,3-h] chromen-9-yl 3-methylbut-2-enoate	metab_20049	C19H20O6	up

Table S5 Liver Metabolomics (continued)

ID	Metabolite	Metab ID	Formula	Regulate
neg_2671	9-Oxo-nonanoic acid	metab_20420	C9H16O3	up
neg_2965	2,2'-(3-methylcyclohexane-1,1-diyl)diacetic acid	metab_20710	C11H18O4	up
neg_3355	(4S,8R)-8,9-Dihydroxy-p-menth-1(6)-en-2-one	metab_21095	C10H16O3	up
neg_3938	3-keto-Digoxigenin	metab_21674	C23H32O5	up
neg_3958	Atractyligenin	metab_21694	C20H30O3	up
neg_4801	5-cis-15(R)-Iloprost	metab_22521	C22H32O4	up
neg_5069	PGA1	metab_22788	C20H32O4	up
neg_5285	17-keto-4(Z),7(Z),10(Z),13(Z),15(E),19(Z)-Docosahexaenoic Acid	metab_22997	C22H30O3	up
neg_10016	Annoglabasin F	metab_27564	C22H34O5	up
neg_10258	Panaquinquecol 1	metab_27799	C18H28O3	up
neg_10972	Arginyl-Tryptophan	metab_28510	C17H24N6O3	up
neg_11214	Annuolide E	metab_28751	C15H20O3	up
neg_11648	6-Pentyl-2H-pyran-2-one	metab_29184	C10H14O2	up
neg_11767	Trans-4,5-epoxy-2(E)-Decenal	metab_29301	C10H16O2	up
neg_11943	Phenylpyruvic acid	metab_29474	C9H8O3	up
neg_12458	Pseudoecgonine	metab_29984	C9H15NO3	up
neg_12732	Isoleucyl-Tyrosine	metab_30257	C15H22N2O4	up
neg_12944	Glycyl-Phenylalanine	metab_30466	C11H14N2O3	up
neg_13029	Leucyl-Arginine	metab_30546	C12H25N5O3	up
neg_13075	Acetyl-DL-Valine	metab_30589	C7H13NO3	up
neg_11757	Dehydrovomifoliol	metab_31296	C13H18O3	up
pos_10	N-Acetyl-DL-methionine	metab_9	C7H13NO3S	up
pos_33	N-Acetyl-L-phenylalanine	metab_32	C11H13NO3	up
pos_54	3-Hydroxy-beta-ionone	metab_53	C13H20O2	up
pos_230	Acetyl-L-tyrosine	metab_229	C11H13NO4	up
pos_275	6E-nonenoic acid	metab_273	C9H16O2	up
pos_281	PC(20:5/0:0)	metab_279	C28H48NO7P	up
pos_1085	2-Pentyl-3-phenyl-2-propenal	metab_1070	C14H18O	up
pos_1716	Glechomafuran	metab_1688	C15H20O3	up
pos_1721	(-)-Leucothol C	metab_1693	C20H30O4	up
pos_1722	5(S),14(R)-Lipoxin B4	metab_1694	C20H32O5	up
pos_2987	5,6-Ep-15S-HETE	metab_2950	C20H30O4	up
pos_3010	Pseudoionone	metab_2973	C13H20O	up
pos_3014	13(S)-HpOTrE	metab_2977	C18H30O4	up
pos_3246	Spermine	metab_3207	C10H26N4	up
pos_4360	ALANYL-dl-PHENYLALANINE	metab_4265	C12H16N2O3	up

Table S5 Liver Metabolomics (continued)

ID	Metabolite	Metab ID	Formula	Regulate
pos_4812	Jasmolone	metab_4711	C11H16O2	up
pos_4891	O-Adipoylcarnitine	metab_4789	C13H23NO6	up
pos_4990	(S)-Neolyratyl acetate	metab_4888	C12H18O2	up
pos_5077	10beta-12,13-Dinor-8-oxo-6-eremophilen-11-al	metab_4975	C13H18O2	up
pos_6717	Thromboxane B3	metab_6608	C20H32O6	up
pos_7059	6alpha-methylprednisolone	metab_6948	C22H30O5	up
pos_7302	Tetrahydrodeoxycortisol	metab_7189	C21H34O4	up
pos_7376	PGD2 ethanolamide	metab_7263	C22H37NO5	up
pos_11803	25-Cinnamoyl-vulgaroside	metab_11567	C34H46O7	up
pos_12232	6,8,10,12-pentadecatetraenal	metab_11993	C15H22O	up
pos_12332	(10)-Gingerol	metab_12093	C21H34O4	up
pos_12850	PGE3 1,15-lactone	metab_12609	C20H28O4	up
pos_13209	12,13-Epoxy-9,15-octadecadienoic acid	metab_12966	C18H30O3	up
pos_13327	Bicyclo-PGE2	metab_13083	C20H30O4	up
pos_13517	5,6,15-trihydroxy-7,9,13-Eicosatrien-11-ynoic acid	metab_13273	C20H30O5	up
pos_13520	16-phenoxy tetranor PGF2alpha	metab_13276	C22H30O6	up
pos_13869	1,2,4-Trimethylbenzene	metab_13624	C9H12	up
pos_13926	2-Phenylethyl octanoate	metab_13681	C16H24O2	up
pos_14272	2-Hydroxyacorenone	metab_14024	C15H24O2	up
pos_14289	20-COOH-leukotriene E4	metab_14041	C23H35NO7S	up
pos_16218	M-Cresol	metab_17833	C7H8O	up

Table S6 RNA-seq

Gene ID	Gene name	Gene description	P_Ctrl_ vs_P_GHB
242			
ENSMUSG00000059089	Fcgr4	Fc receptor, IgG, low affinity IV	down
ENSMUSG00000114133	Gm20075	predicted gene, 20075	down
ENSMUSG00000043740	B430306N03Rik	RIKEN cDNA B430306N03 gene	down
ENSMUSG00000027398	Il1b	interleukin 1 beta	down
ENSMUSG00000009092	Derl3	Der1-like domain family, member 3	down
ENSMUSG00000015854	Cd5l	CD5 antigen-like	down
ENSMUSG00000051736	Fam229b	family with sequence similarity 229	down
ENSMUSG00000044938	Klhl31	kelch-like 31	down
ENSMUSG00000028931	Kcnab2	potassium voltage-gated channel, shaker-related subfamily, beta member 2	down
ENSMUSG00000059994	Fcrl1	Fc receptor-like 1	down
ENSMUSG00000043263	Ifi209	interferon activated gene 209	down
ENSMUSG00000019874	Fabp7	fatty acid binding protein 7	down
ENSMUSG00000023078	Cxcl13	chemokine (C-X-C motif) ligand 13	down
ENSMUSG00000058981	Olfr1406	olfactory receptor 1406	down
ENSMUSG00000045868	Gvin1	GTPase, very large interferon inducible 1	down
ENSMUSG00000031906	Smpd3	sphingomyelin phosphodiesterase 3, neutral	down
ENSMUSG00000029752	Asns	asparagine synthetase	down
ENSMUSG00000115902	D730005E14Rik	RIKEN cDNA D730005E14 gene	down
ENSMUSG00000117079	Gm41611	predicted gene, 41611	down
ENSMUSG00000026390	Marco	macrophage receptor with collagenous structure	down
ENSMUSG00000076612	Ighg2c	immunoglobulin heavy constant gamma 2C	down
ENSMUSG00000076613	Ighg2b	immunoglobulin heavy constant gamma 2B	down
ENSMUSG00000089942	Pira2	paired-Ig-like receptor A2	down
ENSMUSG00000101264	Gm28347	predicted gene 28347	down
ENSMUSG00000096950	Gm9530	predicted gene 9530	down
ENSMUSG00000072761	Gm6712	predicted gene 6712	down
ENSMUSG00000096715	Igkv3-4	immunoglobulin kappa variable 3-4	down
ENSMUSG00000117545	Gm30794	predicted gene, 30794	down
ENSMUSG00000030474	Siglece	sialic acid binding Ig-like lectin E	down
ENSMUSG00000050994	Adgb	androglobin	down
ENSMUSG00000055546	Timd4	T cell immunoglobulin and mucin domain containing 4	down
ENSMUSG00000050022	Amz1	archaelysin family metallopeptidase 1	down

Table S6 RNA-seq (continued)

Gene ID	Gene name	Gene description	P_Ctrl_ vs_P_GHB
ENSMUSG00000062593	Gm49339	predicted gene, 49339	down
ENSMUSG00000037318	Traf3ip3	TRAF3 interacting protein 3	down
ENSMUSG00000087623	Gm12404	predicted gene 12404	down
ENSMUSG00000030054	Gp9	glycoprotein 9 (platelet)	down
ENSMUSG00000022489	Pde1b	phosphodiesterase 1B, Ca2+-calmodulin dependent	down
ENSMUSG00000031304	Il2rg	interleukin 2 receptor, gamma chain	down
ENSMUSG00000103998	Gm38025	predicted gene, 38025	down
ENSMUSG00000031093	Dock11	dedicator of cytokinesis 11	down
ENSMUSG00000056071	S100a9	S100 calcium binding protein A9 (calgranulin B)	down
ENSMUSG00000032254	Kif23	kinesin family member 23	down
ENSMUSG00000112332	4930466K18Rik	RIKEN cDNA 4930466K18 gene	down
ENSMUSG00000034438	Gbp8	guanylate-binding protein 8	down
ENSMUSG00000039533	Mmd2	monocyte to macrophage differentiation-associated 2	down
ENSMUSG00000051439	Cd14	CD14 antigen	down
ENSMUSG00000076609	Igkc	immunoglobulin kappa constant	down
ENSMUSG00000024679	Ms4a6d	membrane-spanning 4-domains, subfamily A, member 6D	down
ENSMUSG00000031506	Ptpn7	protein tyrosine phosphatase, non-receptor type 7	down
ENSMUSG00000078763	Slfn1	schlafen 1	down
ENSMUSG00000035004	Igsf6	immunoglobulin superfamily, member 6	down
ENSMUSG00000098290	Obox4-ps1	oocyte specific homeobox 4, pseudogene 1	down
ENSMUSG00000025930	Msc	musculin	down
ENSMUSG00000078154	Gm12184	predicted gene 12184	down
ENSMUSG00000030278	Cidec	cell death-inducing DFFA-like effector c	down
ENSMUSG00000087273	Gm13203	predicted gene 13203	down
ENSMUSG00000021322	Aoah	acyloxyacyl hydrolase	down
ENSMUSG00000023067	Cdkn1a	cyclin-dependent kinase inhibitor 1A (P21)	down
ENSMUSG00000032484	Ngp	neutrophilic granule protein	down
ENSMUSG00000073207	Ccdc160	coiled-coil domain containing 160	down
ENSMUSG00000076937	Iglc2	immunoglobulin lambda constant 2	down
ENSMUSG00000076934	Iglv1	immunoglobulin lambda variable 1	down
ENSMUSG00000089829	Gm16565	predicted gene 16565	down
ENSMUSG00000059108	Ifitm6	interferon induced transmembrane protein 6	down
ENSMUSG00000038543	BC028528	cDNA sequence BC028528	down

Table S6 RNA-seq (continued)

Gene ID	Gene name	Gene description	P_Ctrl_ vs_P_GHB
ENSMUSG00000024353	Mzb1	marginal zone B and B1 cell-specific protein 1	down
ENSMUSG00000026536	Ifi211	interferon activated gene 211	down
ENSMUSG00000069792	Wfdc17	WAP four-disulfide core domain 17	down
ENSMUSG00000044912	Syt16	synaptotagmin XVI	down
ENSMUSG00000037868	Egr2	early growth response 2	down
ENSMUSG00000040026	Saa3	serum amyloid A 3	down
ENSMUSG00000000392	Fap	fibroblast activation protein	down
ENSMUSG00000036905	C1qb	complement component 1, q subcomponent, beta polypeptide	down
ENSMUSG00000106380	Gm3519	predicted gene 3519	down
ENSMUSG00000030144	Clec4d	C-type lectin domain family 4, member d	down
ENSMUSG00000109209	Gm45104	predicted gene 45104	down
ENSMUSG00000067547	Gm7666	predicted pseudogene 7666	down
ENSMUSG00000020057	Dram1	DNA-damage regulated autophagy modulator 1	down
ENSMUSG00000033777	Tlr13	toll-like receptor 13	down
ENSMUSG00000046182	Gsg1l	GSG1-like	down
ENSMUSG00000030148	Clec4a2	C-type lectin domain family 4, member a2	down
ENSMUSG00000058174	Gm5148	predicted gene 5148	down
ENSMUSG00000064246	Chil1	chitinase-like 1	down
ENSMUSG00000025020	Slit1	slit guidance ligand 1	down
ENSMUSG00000097113	Gm19705	predicted gene, 19705	down
ENSMUSG00000092083	Kcnb2	potassium voltage gated channel, Shab-related subfamily, member 2	down
ENSMUSG00000022432	Smc1b	structural maintenance of chromosomes 1B	down
ENSMUSG00000005667	Mthfd2	methylenetetrahydrofolate dehydrogenase (NAD+ dependent), methenyltetrahydrofolate cyclohydrolase	down
ENSMUSG00000089859	Olfr1565	olfactory receptor 1565	down
ENSMUSG00000052270	Fpr2	formyl peptide receptor 2	down
ENSMUSG00000070806	Zmynd12	zinc finger, MYND domain containing 12	down
ENSMUSG00000055202	Zfp811	zinc finger protein 811	down
ENSMUSG00000048794	Cfap100	cilia and flagella associated protein 100	down
ENSMUSG00000102014	2900009J06Rik	RIKEN cDNA 2900009J06 gene	down
ENSMUSG00000106709	Gm30270	predicted gene, 30270	down
ENSMUSG00000034987	Hrh2	histamine receptor H2	down
ENSMUSG00000036362	P2ry13	purinergic receptor P2Y, G-protein coupled 13	down

Table S6 RNA-seq (continued)

Gene ID	Gene name	Gene description	P_Ctrl_ vs_P_GHB
ENSMUSG00000057425	Ugt2b37	UDP glucuronosyltransferase 2 family, polypeptide B37	down
ENSMUSG00000076552	Igkv4-61	immunoglobulin kappa chain variable 4-61	down
ENSMUSG00000020642	Rnf144a	ring finger protein 144A	down
ENSMUSG00000048498	Cd300e	CD300E molecule	down
ENSMUSG00000034059	Ypel4	yippee like 4	down
ENSMUSG00000028497	Hacd4	3-hydroxyacyl-CoA dehydratase 4	down
ENSMUSG00000113152	Gm48422	predicted gene, 48422	down
ENSMUSG00000029816	Gpnmb	glycoprotein (transmembrane) nmb	down
ENSMUSG00000023992	Trem2	triggering receptor expressed on myeloid cells 2	down
ENSMUSG00000061540	Orm2	orosomucoid 2	down
ENSMUSG00000110047	A230085B16Rik	RIKEN cDNA A230085B16 gene	down
ENSMUSG00000025163	Cd7	CD7 antigen	down
ENSMUSG00000111282	Gm47528	predicted gene, 47528	down
ENSMUSG00000106628	Gm43558	predicted gene 43558	down
ENSMUSG00000066682	Pilrb2	paired immunoglobin-like type 2 receptor beta 2	down
ENSMUSG00000113088	Gm36757	predicted gene, 36757	down
ENSMUSG00000042244	Pglyrp3	peptidoglycan recognition protein 3	down
ENSMUSG00000020798	Spns3	spinster homolog 3	down
ENSMUSG00000087390	Gm7598	predicted gene 7598	down
ENSMUSG00000002699	Lcp2	lymphocyte cytosolic protein 2	down
ENSMUSG00000032224	Fam81a	family with sequence similarity 81, member A	down
ENSMUSG00000030651	Art2b	ADP-ribosyltransferase 2b	down
ENSMUSG00000062488	Ifit3b	interferon-induced protein with tetratricopeptide repeats 3B	down
ENSMUSG00000047798	Cd300lf	CD300 molecule like family member F	down
ENSMUSG00000063838	Cdc42ep5	CDC42 effector protein (Rho GTPase binding) 5	down
ENSMUSG00000026358	Rgs1	regulator of G-protein signaling 1	down
ENSMUSG00000000982	Ccl3	chemokine (C-C motif) ligand 3	down
ENSMUSG00000082776	Gm7061	predicted gene 7061	down
ENSMUSG00000113790	Gm17872	predicted gene, 17872	down
ENSMUSG00000059775	Rps26-ps1	ribosomal protein S26, pseudogene 1	down
ENSMUSG00000030708	Dnajb13	DnaJ heat shock protein family (Hsp40) member B13	down
ENSMUSG00000020431	Adcy1	adenylate cyclase 1	down

Table S6 RNA-seq (continued)

Gene ID	Gene name	Gene description	P_Ctrl_ vs_P_GHB
ENSMUSG00000021904	Sema3g	sema domain, immunoglobulin domain (Ig), short basic domain, secreted, (semaphorin) 3G	down
ENSMUSG00000049107	Ntf3	neurotrophin 3	down
ENSMUSG00000032816	Igdcc4	immunoglobulin superfamily, DCC subclass, member 4	down
ENSMUSG00000024056	Ndc80	NDC80 kinetochore complex component	down
ENSMUSG00000022876	Samsn1	SAM domain, SH3 domain and nuclear localization signals, 1	down
ENSMUSG00000035373	Ccl7	chemokine (C-C motif) ligand 7	down
ENSMUSG00000072620	Slfn2	schlafen 2	down
ENSMUSG00000052013	Btla	B and T lymphocyte associated	down
ENSMUSG00000057182	Scn3a	sodium channel, voltage-gated, type III, alpha	down
ENSMUSG00000038085	Cnbd2	cyclic nucleotide binding domain containing 2	down
ENSMUSG00000060402	Chst8	carbohydrate sulfotransferase 8	down
ENSMUSG00000087611	4930458D05Rik	RIKEN cDNA 4930458D05 gene	down
ENSMUSG00000079293	Clec7a	C-type lectin domain family 7, member a	down
ENSMUSG00000090164	BC035044	cDNA sequence BC035044	down
ENSMUSG00000064147	Rab44	RAB44, member RAS oncogene family	down
ENSMUSG00000110316	Gm45311	predicted gene 45311	down
ENSMUSG00000038917	3930402G23Rik	RIKEN cDNA 3930402G23 gene	down
ENSMUSG00000030650	Tmc5	transmembrane channel-like gene family 5	down
ENSMUSG00000010461	Eya4	EYA transcriptional coactivator and phosphatase 4	down
ENSMUSG00000024521	Pmaip1	phorbol-12-myristate-13-acetate-induced protein 1	down
ENSMUSG00000084319	Tpt1-ps3	tumor protein, translationally-controlled, pseudogene 3	down
ENSMUSG00000024008	Cpne5	copine V	down
ENSMUSG00000015950	Ncf1	neutrophil cytosolic factor 1	down
ENSMUSG00000105504	Gbp5	guanylate binding protein 5	down
ENSMUSG00000020892	Aloxe3	arachidonate lipoxygenase 3	down
ENSMUSG00000051627	H1f4	H1.4 linker histone, cluster member	down
ENSMUSG00000024013	Fgd2	FYVE, RhoGEF and PH domain containing 2	down
ENSMUSG00000024399	Ltb	lymphotoxin B	down
ENSMUSG00000040264	Gbp2b	guanylate binding protein 2b	down
ENSMUSG00000004359	Spic	Spi-C transcription factor (Spi-1/PU.1 related)	down
ENSMUSG00000105055	Gm43079	predicted gene 43079	down
ENSMUSG00000028555	Ttc39a	tetratricopeptide repeat domain 39A	down

Table S6 RNA-seq (continued)

Gene ID	Gene name	Gene description	P_Ctrl_ vs_P_GHB
ENSMUSG00000020573	Pik3cg	phosphatidylinositol-4,5-bisphosphate 3-kinase catalytic subunit gamma	down
ENSMUSG00000044708	Kcnj10	potassium inwardly-rectifying channel, subfamily J, member 10	down
ENSMUSG00000071661	Zbtb3	zinc finger and BTB domain containing 3	down
ENSMUSG00000017652	Cd40	CD40 antigen	down
ENSMUSG00000046167	Gldn	gliomedin	down
ENSMUSG00000086481	Gm11707	predicted gene 11707	down
ENSMUSG00000085014	Gm13490	predicted gene 13490	down
ENSMUSG00000023349	Clec4n	C-type lectin domain family 4, member n	down
ENSMUSG00000050335	Lgals3	lectin, galactose binding, soluble 3	down
ENSMUSG00000072596	Ear2	eosinophil-associated, ribonuclease A family, member 2	down
ENSMUSG00000020218	Wif1	Wnt inhibitory factor 1	down
ENSMUSG00000044811	Cd300c2	CD300C molecule 2	down
ENSMUSG00000060044	Tmem26	transmembrane protein 26	down
ENSMUSG00000069516	Lyz2	lysozyme 2	down
ENSMUSG00000004730	Adgre1	adhesion G protein-coupled receptor E1	down
ENSMUSG00000003545	Fosb	FBJ osteosarcoma oncogene B	down
ENSMUSG00000026068	Il18rap	interleukin 18 receptor accessory protein	down
ENSMUSG00000076614	Ighg1	immunoglobulin heavy constant gamma 1 (G1m marker)	down
ENSMUSG00000036353	P2ry12	purinergic receptor P2Y, G-protein coupled 12	down
ENSMUSG00000038642	Ctss	cathepsin S	down
ENSMUSG00000104077	Gm37027	predicted gene, 37027	down
ENSMUSG00000060176	Kif27	kinesin family member 27	down
ENSMUSG00000095351	Igkv3-2	immunoglobulin kappa variable 3-2	down
ENSMUSG00000018927	Ccl6	chemokine (C-C motif) ligand 6	down
ENSMUSG00000074342	I830077J02Rik	RIKEN cDNA I830077J02 gene	down
ENSMUSG00000044229	Nxpe4	neurexophilin and PC-esterase domain family, member 4	down
ENSMUSG00000097391	Mirg	miRNA containing gene	down
ENSMUSG00000103037	Pcdhgb1	protocadherin gamma subfamily B, 1	down
ENSMUSG00000030200	Bcl2l14	BCL2-like 14 (apoptosis facilitator)	down
ENSMUSG00000025165	Sectm1a	secreted and transmembrane 1A	down
ENSMUSG00000022148	Fyb	FYN binding protein	down

Table S6 RNA-seq (continued)

Gene ID	Gene name	Gene description	P_Ctrl_ vs_P_GHB
ENSMUSG00000049625	Tifab	TRAF-interacting protein with forkhead-associated domain, family member B	down
ENSMUSG00000020808	Pimreg	PICALM interacting mitotic regulator	down
ENSMUSG00000044827	Tlr1	toll-like receptor 1	down
ENSMUSG00000032739	Pram1	PML-RAR alpha-regulated adaptor molecule 1	down
ENSMUSG00000074183	Gsta1	glutathione S-transferase, alpha 1 (Ya)	down
ENSMUSG00000024300	Myo1f	myosin IF	down
ENSMUSG00000039013	Siglecf	sialic acid binding Ig-like lectin F	down
ENSMUSG00000110498	A630001O12Rik	RIKEN cDNA A630001O12 gene	down
ENSMUSG00000062007	Hsh2d	hematopoietic SH2 domain containing	down
ENSMUSG00000064358	mt-Co3	mitochondrially encoded cytochrome c oxidase III	up
ENSMUSG00000096497	Olfr787	olfactory receptor 787	up
ENSMUSG00000110099	Gm45344	predicted gene 45344	up
ENSMUSG00000031517	Gpm6a	glycoprotein m6a	up
ENSMUSG00000043753	Dmrta1	doublesex and mab-3 related transcription factor like family A1	up
ENSMUSG00000095486	Vmn2r22	vomeronasal 2, receptor 22	up
ENSMUSG00000106447	Gm42957	predicted gene 42957	up
ENSMUSG00000082762	Gm12366	predicted gene 12366	up
ENSMUSG00000055271	9330161L09Rik	RIKEN cDNA 9330161L09 gene	up
ENSMUSG00000085101	Platr16	pluripotency associated transcript 16	up
ENSMUSG00000109953	5430430B14Rik	RIKEN cDNA 5430430B14 gene	up
ENSMUSG00000037096	Gm9762	predicted pseudogene 9762	up
ENSMUSG00000112008	Gm47218	predicted gene, 47218	up
ENSMUSG00000081671	Gm13167	predicted gene 13167	up
ENSMUSG00000028546	Elavl4	ELAV like RNA binding protein 4	up
ENSMUSG00000106767	Gm42727	predicted gene 42727	up
ENSMUSG00000051022	Hs3st1	heparan sulfate (glucosamine) 3-O-sulfotransferase 1	up
ENSMUSG00000040537	Adam22	a disintegrin and metallopeptidase domain 22	up
ENSMUSG00000109564	Muc16	mucin 16	up
ENSMUSG00000023039	Krt7	keratin 7	up
ENSMUSG00000115782	Gm49116	predicted gene, 49116	up
ENSMUSG00000105912	Gm10440	predicted gene 10440	up
ENSMUSG00000024274	Zscan30	zinc finger and SCAN domain containing 30	up

Table S6 RNA-seq (continued)

Gene ID	Gene name	Gene description	P_Ctrl_ vs_P_GHB
ENSMUSG00000047155	Cyp4x1	cytochrome P450, family 4, subfamily x, polypeptide 1	up
ENSMUSG00000074796	Slc4a11	solute carrier family 4, sodium bicarbonate transporter-like, member 11	up
ENSMUSG00000041730	Prrxl1	paired related homeobox protein-like 1	up
ENSMUSG00000086916	Gm15903	predicted gene 15903	up
ENSMUSG00000042985	Upk3b	uroplakin 3B	up
ENSMUSG00000112516	Gm47968	predicted gene, 47968	up
ENSMUSG00000097760	6030442K20Rik	RIKEN cDNA 6030442K20 gene	up
ENSMUSG00000063011	Msln	mesothelin	up
ENSMUSG00000071347	C1qtnf9	C1q and tumor necrosis factor related protein 9	up
ENSMUSG00000087367	Gm15491	predicted gene 15491	up
ENSMUSG00000049436	Upk1b	uroplakin 1B	up
ENSMUSG00000081855	Rpl17-ps5	ribosomal protein L17, pseudogene 5	up
ENSMUSG00000023935	Spats1	spermatogenesis associated, serine-rich 1	up
ENSMUSG00000111539	Gm48372	predicted gene, 48372	up
ENSMUSG00000107227	Gm42559	predicted gene 42559	up
ENSMUSG00000103400	Gm15853	predicted gene 15853	up
ENSMUSG00000023046	Igfbp6	insulin-like growth factor binding protein 6	up
ENSMUSG00000005237	Dnah2	dynein, axonemal, heavy chain 2	up